Floral Stage Optimization and Immune Evasion Enhance *Agrobacterium*-Mediated Genome Editing in *Arabidopsis*

Running title: Innovative approaches for *Agrobacterium*-Mediated Genome Editing

Mao-Sen Liu[†], Teng-Kuei Huang[†], Yi-Chieh Wang, Si-Chong Wang, Chih-Hang Wu, Chih-Horng Kuo, Erh-Min Lai*

Institute of Plant and Microbial Biology, Academia Sinica, Taipei, Taiwan

*Correspondence (Tel: +886-2-2787-1158; email: emlai@gate.sinica.edu.tw)

[†]These authors contributed equally to this work

Author details, including affiliation and email address

msliu@gate.sinica.edu.tw; tengkueih@gmail.com; ejw@gate.sinica.edu.tw; sky972sakura@gmail.com; wuchh@gate.sinica.edu.tw; chk@gate.sinica.edu.tw; emlai@gate.sinica.edu.tw

ORCID ID

ORCID ID of the authors: M.-S.L. 0000-0003-0324-5866; T.-K.H. 0000-0001-7369-3678; S.-C.W. 0000-0002-6192-8844; C.-H.W. 0000-0003-1616-1872; C.-H.K. 0000-0002-2857-0529; E.-M.L. 0000-0003-3630-8683

Word counts: 5377 words (Introduction, Materials and Methods, Results, Discussion)

Number of figures: 7 (all to be published in colour)

Supporting information

SUMMARY

- *Agrobacterium*-mediated transformation via floral inoculation (AMT-FI) enables genetic engineering without tissue culture. It is widely used in the model plant *Arabidopsis thaliana*, yet its efficiency and broader applicability remain limited.
- Here, we used a dual-reporter system (RUBY and hygromycin resistance) to identify key floral stages and engineered *Agrobacterium* strains to evade plant immunity, leading to enhanced transient expression and genome editing.
- We determined flowers opened at 6 days post-inoculation (DPI) are optimal for high transformation efficiency, with nearly 100% of siliques harboring transformants. However, *Agrobacterium* infection induced ovule abortion, particularly in wild-type (Col-0) plants, whereas *efr* mutants lacking the EF-Tu receptor (EFR)-mediated pattern-triggered immunity (PTI) showed reduced ovule abortion. Notably, *efr* mutants exhibited more RUBY-positive ovules and significantly enhanced genome editing efficiency. Two engineered stealth *Agrobacterium* strains (AS201 and AS202) expressing a chimeric EF-Tu for evading recognition by EFR enhanced both transient transformation and genome editing efficiency. Remarkably, genome-edited T1 plants could be recovered based on phenotype or direct sequencing without the need for antibiotic selection when targeting flowers opened at 6 DPI.
- By integrating floral stage selection, immune evasion, and *Agrobacterium* engineering, this study provides a practical and versatile platform to advance plant genome engineering.

KEY WORDS

Arabidopsis, *Agrobacterium*, floral dip, plant immunity, genome editing, *Agrobacterium*-mediated transformation, EF-Tu, EFR

INTRODUCTION

Agrobacterium species are unique bacteria capable of cross-kingdom gene transfer, leading to diseases like crown gall or hairy root in a wide range of plant species (Hwang *et al.*, 2017; Lacroix & Citovsky, 2019). This remarkable ability has been harnessed in plant genetic engineering by replacing the oncogenes within T-DNA region of tumor-inducing plasmids with genes of interest (Suzuki *et al.*, 2009; Hooykaas, 2023). *Agrobacterium*-mediated transformation (AMT) has become a cornerstone technique in plant biology and the development of genetically modified organisms (GMOs) that stably express agricultural traits for crop improvements (Bevan, 1984; Gelvin, 2003).

Beyond enabling stable gene integration, AMT also supports transient expression of genome-editing machinery, allowing precise genome modifications. Since the T-DNA containing these editing components can be eliminated via chromosome segregation in subsequent generations, this strategy mitigates food safety concerns associated with GMOs (Pixley *et al.*, 2022).

Agrobacterium naturally infects somatic plant cells by responding to wound signals in roots or stems. Interestingly, it can also target germline tissues such as female gametophytes, which laid the foundation for the floral dip method widely used in *Arabidopsis thaliana* (Clough & Bent, 1998; Angulo *et al.*, 2023). This method, referred to here as *Agrobacterium*-mediated transformation by floral inoculation (AMT-FI), bypasses labor-intensive tissue culture, offering a more efficient transformation pathway. However, its application in species beyond *A. thaliana* has limited success (Bélanger *et al.*, 2024).

Although many plant factors that promote or suppress tumorigenesis and AMT have been identified, the genes involved in AMT-FI appear to be distinct (Hwang *et al.*, 2017; Lacroix & Citovsky, 2019; Weisberg *et al.*, 2023). Several *Arabidopsis* mutants or ecotypes resistant to root transformation remain susceptible to AMT-FI (Nam *et al.*, 1997; Mysore *et al.*, 2000). Notably, *polQ* mutants lacking DNA polymerase theta are completely deficient in T-DNA integration via AMT-FI but retain capability for stable transformation in roots, albeit at lower efficiencies (van Kregten *et al.*, 2016; Nishizawa-Yokoi *et al.*, 2021). These findings highlight fundamental mechanistic

differences between AMT in germline and somatic cells. Understanding the genetic and molecular basis of AMT-FI is crucial to expanding its utility across plant species.

Plant immunity plays a pivotal role in suppressing tumorigenesis and AMT efficiencies (Tiwari *et al.*, 2022; Dodds *et al.*, 2024). Upon *Agrobacterium* infection, plants recognize pathogen-associated molecular patterns (PAMPs) such as EF-Tu, flagellin, and cold-shock proteins by pattern-recognition receptors (PRRs), activating pattern-triggered immunity (PTI) that suppress transformation (Zipfel *et al.*, 2006; Wu *et al.*, 2014; Saur *et al.*, 2016; Wang *et al.*, 2018; Fürst *et al.*, 2020). Salicylic acid (SA) is a key defense hormone that reduces tumor formation and transient transformation (Anand *et al.*, 2008). Additionally, antimicrobial secondary metabolites, including glucosinolates and camalexin, restrict *Agrobacterium* infection at early and late stages, respectively (Shih *et al.*, 2018). These defense strategies collectively highlight the resilience of plants to counteract *Agrobacterium* infection and limit its transformation success.

In *Arabidopsis*, the EF-Tu receptor (EFR) plays a key role in recognizing *Agrobacterium* EF-Tu and inhibiting transient transformation (Zipfel *et al.*, 2006; Wu *et al.*, 2014; Wang *et al.*, 2018). However, the impact of EFR-mediated PTI on stable transformation remains obscure (van Tol *et al.*, 2022). Moreover, its influence on AMT-FI-mediated genome editing has not been fully elucidated. Although a recent study used *A. thaliana efr* mutants to investigate this question, conclusive evidence is lacking (van Tol *et al.*, 2022).

In this study, we investigated the temporal and spatial localization of *Agrobacterium* cells and transformation events during AMT-FI in *A. thaliana.* A dual reporter system, combining a visible RUBY marker with a hygromycin resistance marker, was utilized to identify the floral tissues and stages most susceptible to AMT. Furthermore, we examined the impact of EFR-mediated PTI in transformation and genome-editing efficiencies. Our results revealed that AMT events peak in flowers open at 6 days post-inoculation (DPI), with *efr* mutants exhibiting significantly higher genome editing efficiency than Col-0. Moreover, we engineered two independent *Agrobacterium* strains expressing a chimeric EF-Tu, which further enhanced both transient expression and genome editing efficiency without significantly altering stable

transformation frequency. These findings offer new strategies to facilitate AMT-FI-based genome editing in plants.

MATERIALS AND METHODS

Plant materials and growth condition

Arabidopsis thaliana Col-0, EF-Tu receptor (EFR) mutants, *efr*-1 (SALK_044334) and *efr*-2 (SALK_068675) were used in this study. Seeds were sown in soil (peatmoss:vermiculite:perlite = 12:1:1), germinated, and grown in a growth room under conditions of 22 °C with 16h light/8h dark photoperiod.

Bacterial growth condition

For tracking *Agrobacterium* localization and transformation events, *Agrobacterium* cells were cultured in 523 with appropriate antibiotics (Kado & Heskett, 1970). For genome editing experiments, LB medium supplemented with appropriate antibiotics was used. Freshly streaked out *Agrobacterium* colonies grown on 523 or LB agar were cultured in the same medium (5 mL) for 2 days at 28 °C. The cultures were subsequently diluted 1:1000 in 50 mL 523 or LB, grown for 22-24 hours, harvested by centrifugation at 6000x g for 20 minutes. The cell pellets were resuspended in infiltration medium (1/2 MS, 5% sucrose, 0.04% silwet-L77, 44 nM BAP and 200 μM AS, pH=5.7) to OD_{600}=1.

Plasmid construction

Plasmid and primer information are listed in Table S1 and S2, respective. 35S::RUBY plasmid (Addgene#160908) which provided a visible RUBY reporter and hygromycin resistance reporter was obtained from Addgene.

The gentamycin resistance gene (Gen^R) of pRL662-GFP(S65T) (Yu *et al.*, 2021) was replaced by spectinomycin resistance gene from 35S::RUBY to obtain pRL662-GFP(S65T)/Spe^R by use of Gibson Assembly® Master Mix (New England Biolabs, USA). mCherry2 with a 3'-end nuclear localization signal (mCherry-NLS) was generated from pEB2-2ndVal mCherry2-L (Addgene#104027) by PCR. PCR was performed by use of KAPA HiFi HotStart ReadyMix PCR Kit (KapaBiosystems, South Africa) and PCR products were cloned into the pJet1.2/blunt plasmid following

149 the user manual of CloneJET PCR Cloning Kit (ThermoFisher Scientific, USA).
150 35S::mCherry2-SV40/Kan^{R} binary vector was constructed with Golden Gate
151 Assembly.

152 A3A-CBE coding region was amplified from pYPQ265E2 (Addgene #164719) and
153 was subcloned into XbaI/SacI digested pHEE901 (Addgene #91707) via Gibson
154 Assembly. Protospacers were cloned into pA3A-CBE vectors as previously
155 described (Steinert *et al.*, 2015). To generate the *tufAB*$^{Pst4\text{-}15}$ mutants in GV3101, we
156 employed double crossover vector using pEML041003-tufAPst4-15 and pEML41003-
157 tufBPst4-15. Two 2.5-kb DNA fragments of modified *tufA* and *tufB* were amplified by
158 two pairs of primers, and cloned into pEML041003 by BsaI digestion. AS201 was
159 generated by modifying *tufB* followed by *tufA*, while AS202 was *tufA* followed by
160 *tufB*. In both constructs, the amino acids at positions 4-15 of EF-Tu were substituted
161 from the native sequence SKFERNKPHVNI to the *Pseudomonas syringae* variant
162 EKFDRSLPHCNV.

163 **Seedling transient transformation and GUS activity assays**

164 *A. thaliana* seedling transient expression assay was performed by the AGROBEST
165 (*Agrobacterium*-mediated enhanced seedling transformation) method as previously
166 described, with minor modification (Wu *et al.*, 2014). *Agrobacterium* cultures were
167 adjusted to an OD_{600}=0.01 in AB-MES medium for co-culture with seedlings. Infected
168 seedlings were collected for GUS activity assays after 2.5 days post-inoculation.

169 ***Agrobacterium*-mediated transformation by floral inoculation (AMT-FI)**

170 AMT-FI was performed according to the published procedure (Clough & Bent, 1998)
171 with modifications. For tracking *Agrobacterium* cells and transformation events, each
172 *Arabidopsis* plant was grown in a small pot (5 cm upper diameter x 5 cm high x 3.5
173 cm bottom diameter). For genome editing experiments, three plants were grown in a
174 large pot (7.8 cm upper diameter x 7.8 cm high x 5.7 cm bottom diameter). Plants
175 were grown until they reached ~5 weeks old, with primary inflorescences reaching
176 10 to 15 cm tall. The primary inflorescence was then removed to promote the
177 emergence of secondary inflorescences over the next 5 to 6 days. Immediately prior
178 to floral dipping, all open flowers were removed. Inflorescences were submerged in
179 *Agrobacterium*-containing infiltration medium for 40 seconds, then plants were laid
180 horizontally in trays, covered with plastic film to maintain high humidity, kept in the

181 dark and incubated for 20 to 24 hrs. Plants were returned to the growth room under
182 the same growth condition.

183 For time-course experiments, newly opened flowers were labeled daily following
184 inoculation. GFP-labeled *Agrobacterium* cells and mCherry2 T-DNA reporter signals
185 were examined in ovaries using a Zeiss LSM 510 Meta confocal microscope

186 RUBY signals were monitored visually in plants transformed with GV3101 carrying
187 the 35S::RUBY construct, assisted by a stereo microscope. A Zeiss Lumar V12
188 stereo fluorescent microscope was used to capture images of floral organs,
189 developing ovules, seeds, and seedlings.

190 To evaluate AMT-FI efficiency by RUBY marker, siliques from RUBY-transformed
191 plants were collected daily. To assess stable transformation efficiency, seeds were
192 sterilized in 70% ethanol for 10 min and plated on a 1/2 MS medium supplemented
193 with 25 mg/L hygromycin. The number of germinated seedlings and Hyg^R seedlings
194 was recorded. AMT-FI efficiency was determined based on the proportion of Hyg^R
195 seedlings relative to the total number of germinated seedlings.

196 **Assessment of genome editing efficiency**

197 To simultaneously measure the genome editing and AMT-FI efficiency, seeds from
198 plants transformed with a binary vector carrying a T-DNA-encoded base editor, a
199 sgRNA and a hygromycin resistance gene were surface sterilized and germinated on
200 a 1/2 MS medium supplemented with either 5 mg/L tribenuron or 25 mg/L
201 hygromycin, both containing 100 mg/L timentin. After seven days, the numbers of
202 tribenuron-resistant, hygromycin-resistant, and albino T1 seedlings were recorded.
203 AMT-FI efficiency was estimated using a weight-based approach, assuming 10 mg
204 of seeds equals approximately 500 seeds.

205 **Statistical analysis**

206 An unpaired two-tailed Student's *t*-test, performed using GraphPad Prism 10, was
207 used to assess statistical differences either between Col-0 WT and *efr* mutants or
208 across time-course datasets.

209

210 **RESULTS**

211 ***Agrobacterium* enters the female reproductive organ within one hour but**
212 **transformation events occur in open flowers after five days post inoculation**

213 Although transformation is thought to occur when the female gametophyte becomes
214 accessible, direct links between floral stage and transformation success remain
215 unclear. To investigate the spatial and temporal dynamics of *Agrobacterium* infection
216 and transformation, we engineered a fluorescently labeled *Agrobacterium* strain for
217 live tracking. *Agrobacterium* GV3101 carrying the disarmed Ti plasmid pMP90
218 (hereafter referred as GV3101), constitutively expressing GFP marker and a T-DNA
219 expressed mCherry2, was used for floral inoculation in *A. thaliana* Col-0 (Fig.1a, 1b).
220 GFP-expressing *Agrobacterium* cells were observed as early as 1 hour post-
221 inoculation (HPI) in the early developmental stage of open gynoecia, the female
222 reproductive organ lacking central placenta tissue (Fig. 1c) but were not detected in
223 the later stage of gynoecia containing central placenta tissue (Fig. 1d). This implied
224 that developing placenta may act as a physical barrier to *Agrobacterium* entry during
225 early infection. By 6 HPI, *Agrobacterium* cells accumulated in the locule of open
226 gynoecia (Fig. 1e, 1f), whereas no signal was seen in closed gynoecia (Fig. 1g). This
227 indicated that open gynoecia serve as the main entry point of *Agrobacterium* into the
228 locule before development of female gametophyte.

229 At one day post-inoculation (DPI, Fig. S1), *Agrobacterium* cells were detected in
230 locules of younger, closed gynoecia (Fig. 1h) but were absent in older gynoecia
231 undergoing ovule development (Fig. 1i). All the 13 open gynoecia observed at 6 HPI
232 and 1 DPI showed detectable GFP signals in the locule, indicating the entrance of
233 *Agrobacterium* prior to the closure of gynoecia. At 3 DPI, *Agrobacterium* persisted in
234 the locules of more mature gynoecia (Fig. 1j), and at 5 DPI, just prior to floral open
235 (anthesis), *Agrobacterium* cells were enriched around the micropyles, the ovular
236 opening through which the pollen tube and possibly *Agrobacterium* gain access (Fig.
237 1k). Despite the sustained presence of *Agrobacterium*, successful T-DNA expression
238 indicated by mCherry2 fluorescence was not detected before anthesis (Fig. 1c-k).
239 Similarly, the RUBY reporter signal was absent in gynoecial tissues until after flower
240 opening (Fig. 2c). Following anthesis, mCherry2 signals became visible in cells
241 adjacent to the egg cell/zygote and in the micropyle region where *Agrobacterium*
242 cells had accumulated (Fig. 1l, 1m). Transformation signals were also detected in the
243 integument, the ovule's outer protective layer (Fig. 1m).

Together, these observations reveal that while *Agrobacterium* rapidly enters the open gynoecium as early as 1 HPI, transformation events are temporally restricted, becoming detectable only in flowers open from 5 DPI onward. This correlates with key developmental transitions in ovule accessibility and gametophyte maturity.

RUBY-based reporter system uncovers transformation dynamics and floral abnormalities

The current method for quantifying transformation efficiency of AMT-FI primarily relies on the use of antibiotic resistance genes, using survival rates of T1 seedlings as a proxy for transformation efficiency. However, this approach overlooks transient transformation events that occur at early stages post-inoculation. To better capture both the transient and stable transformation events, we developed a dual-reporter system combining the visible RUBY marker with a hygromycin resistance gene (Fig. 3a).

We first assessed the floral organs exhibiting RUBY expression. The earliest detection of RUBY signals was observed at 4 DPI, localized at the sepals of floral buds (Fig. 2a). By 5 DPI, RUBY expression appeared on the stigma of open flowers but not on pollen grains (Fig. 2b). Dissection of the ovaries revealed RUBY signal in the transmitting tissues (Fig. 2c), as well as in ovules and developing seeds (Fig. 2d, 2e). While many RUBY ovules were abortive (Fig. 2d), others continued to develop normally (Fig. 2e). Most flowers developed and opened normally (Fig. 2f) while a minor subset exhibited developmental abnormalities. These included flowers with partially open petals (Fig. 2g) and those where only the gynoecium emerged from the sepals (Fig. 2h). In mature seeds, RUBY expression ranged in intensity from light pink to dark purple (Fig. 2i), indicating variable expression levels.

In the hygromycin resistance assay, most hygromycin-resistant seedlings only showed weak or sparse RUBY signals, with ~10% or less of T1 seedling showing RUBY in whole seedlings (Fig. S2). Because hygromycin-sensitive seedlings can continue to grow for up to seven days before growth arrest due to their inability to form roots on hygromycin-containing medium, we can still observe $RUBY^{+}/Hyg^{S}$ seedlings, although their frequency is low (less than 1% of total transformants, Fig. 2j). Consequently, not all hygromycin-resistant plants exhibited uniform RUBY expression throughout the plants (Fig. 2k).

Collectively, the dual-reporter system offers a more comprehensive and sensitive tool for monitoring transformation events across the reproductive tissues. The RUBY reporter revealed that AMT-FI enables transformation in a variety of tissues within the female reproductive organ. However, it also uncovered associated developmental abnormalities in flowers and ovules, which in some cases prevent transformed ovules from developing into viable seeds.

Agrobacterium infection and EFR-mediated immunity synergistically disrupt ovule development and seed viability

Since transformation events were only observed in ovaries after anthesis, we sought to trace the occurrence of AMT events in developing siliques using RUBY reporter as a marker (Fig. 3a). Flowers that opened between 1 to 10 DPI were labeled daily. Once embryos were fully developed, approximately 10 days after floral opening and pollination (Baud *et al.*, 2002), each corresponding silique was examined for RUBY signals in ovules/developing seeds.

To assess the impact of EFR-mediated immunity on AMT-FI efficiency, we compared transformation efficiency in Col-0 wild-type (WT) plants and two EFR loss-of-function mutants (*efr*-1 and *efr*-2). Transformation events were primarily detected in flowers that opened between 5 to 9 DPI, with the highest frequency, nearly 100% of siliques showing RUBY-positive ovules in flowers opened at 6 DPI in both Col-0 WT and *efr* mutants (Fig 3b). The percentage of siliques harboring RUBY ovules did not differ significantly between WT and *efr*, suggesting that *Agrobacterium* can access the open gynoecium and subsequently transform ovules with comparable success across genotypes. However, the proportion of RUBY-positive ovules per silique was moderately higher in *efr* mutants, suggesting that compromising EFR-mediated PTI can enhance transformation efficiencies (Fig. 3c. Fig. S3a, S3b). Importantly, the number of siliques per plant and total seed number did not show significant difference between WT and *efr* mutants (Fig. S4). Thus, the higher RUBY transformation rate per silique in *efr* mutants (Fig. 3c, S3b) is not caused by variation of siliques or seeds between Col-0 and *efr* mutant plants.

Given that AMT-FI often induced floral abnormalities and ovule abortion, we further investigated whether EFR-mediated PTI affects ovule viability. Strikingly, in Col-0 WT, nearly 60% of RUBY-positive ovules were abortive, indicating a strong negative

308 impact of AMT-FI on ovule development. In *efr* mutants, although ovule abortion still
309 occurred, the rate was significantly reduced to ~45%. In contrast, fewer than 20% of
310 non-RUBY ovules were abortive, with no significant difference between Col-0 WT
311 and *efr* mutants (Fig. 3d). On average, *Agrobacterium* infection resulted in an ovule
312 abortive rate of ~35% (Fig. 3d, Fig. S3c).

313 Notably, a strong negative correlation was observed between transformation rate
314 and seed viability. Flowers that opened at 6 DPI, despite showing the highest AMT-
315 FI efficiency, produced low number of viable seeds (Fig. 4a), likely due to the high
316 abortion rate of RUBY-positive ovules (Fig. 3d). However, *efr* mutants produced
317 significantly more viable seeds per silique than Col-0 WT from flowers that opened at
318 6 to 8 DPI (Fig. 4a), supporting a role for EFR-mediated immunity in transformation-
319 associated ovule abortion.

320 To determine whether the increased number of viable seeds per silique in *efr*
321 mutants is a consequence of AMT-FI, we quantified seed production in plants treated
322 with infiltration medium, and those inoculated with *Agrobacterium* GV3101 (Fig. S5).
323 Under both conditions, *efr* mutants produced more seeds per silique than Col-0 WT
324 (Fig. S5a, S5b). However, *Agrobacterium* infection further reduced seed numbers in
325 both genotypes. To assess seed viability, we evaluated germination rates. Seeds
326 from plants treated with infiltration medium germinated at nearly 100% but the
327 germination rate is reduced in both Col-0 and *efr* (~90%) with *Agrobacterium*
328 infection. However, when the number of developed/germinated seeds following
329 *Agrobacterium* infection is normalized to that of seeds treated with infiltration
330 medium, *efr* mutants exhibited higher seed development and germination rates (Fig.
331 S5a).

332 Taken together, the results suggested that the elevated abortion rates and reduced
333 seed viability observed here are largely attributable to *Agrobacterium* infection
334 because ovule abortion rates are typically less than 1% under normal growth
335 conditions (van Tol *et al.*, 2022). EFR-mediated immunity may also reduce seed
336 development and viability but pathogen-induced stress from *Agrobacterium* infection
337 has a more substantial negative impact than through EFR alone. While alleviation of
338 EFR-mediated immunity reduced the abortion rate among transformed ovules by
339 ~15%, it did not restore ovule viability to levels observed in non-transformed ovules
340 (Fig. 3d). These findings suggest that, in addition to EF-Tu PAMP recognition, other

341 *Agrobacterium*-derived factors likely contribute to ovule developmental disruption
342 during AMT-FI.

343 **Temporal profiling reveals the optimal window for stable AMT-FI**
344 **transformation**

345 Although the RUBY-positive ovules indicate transformation events, not all develop
346 into viable transgenic T1 seeds. To more accurately evaluate inherited
347 transformation efficiency, we quantified the number of viable transgenic seeds per
348 silique and stable transformation rate using hygromycin resistance (Hyg^R) as a
349 selection marker. Stable transformation efficiency was calculated based on the
350 number and percentage of Hyg^R seedlings collected daily from flowers opened at 5-9
351 DPI (Fig. 4).

352 As expected, siliques from flowers opened at 6 DPI exhibited the highest
353 transformation efficiency, with an average of ~90% and a peak at 100% of siliques
354 containing one or multiple Hyg^R transformants (Fig. 4b). Consistently, stable
355 transformation efficiency peaked at this time point, with an average of ~26% and a
356 peak at 40% of T1 progeny exhibiting hygromycin resistance (Fig. 4c). The number
357 of T1 Hyg^R transformants per plant also reached its highest at 6 DPI, averaging ~55
358 and peaking at 100 per plant (Fig. 4d).

359 These results highlight that flowers opened at 6 DPI as the optimal floral stage for
360 achieving the highest frequency of stable AMT-FI-mediated transformation in
361 *Arabidopsis*.

362 **EFR-mediated immunity suppresses genome editing efficiency**

363 Although no significant increase in stable transformation efficiency was observed in
364 *efr* mutants compared to Col-0 WT (Fig. 3c), previous studies have shown that *efr*
365 mutants exhibit enhanced *Agrobacterium*-mediated transient expression (Zipfel et
366 al., 2006; Wu, Liu et al., 2014). Since transient expression of CRISPR/Cas9
367 components is sufficient to induce genome editing without stable T-DNA integration,
368 we next investigated whether EFR-mediated immunity contributes to gene editing
369 efficiency during AMT-FI.

370 W constructed a T-DNA vector carrying dual selection markers: a hygromycin
371 resistance gene for selecting transgenic plants and a CRISPR/Cas9 system

372 targeting the *ALS* gene, which confers dominant herbicide resistance (Chen *et al.*,
373 2017), for identifying genome-edited plants (Fig. 5a). Given that the egg-cell is a
374 major target of AMT-FI (Desfeux *et al.*, 2000), we adopted a strategy that enables
375 editing in monoploid germline cells at early developmental stages. Specifically, we
376 applied an egg-cell-specific promoter previously shown to induce heritable mutations
377 in the T1 generation (Wang *et al.*, 2015). To enhance genome editing efficiency and
378 streamline the screening process, we employed an A3A/Y130F-CBE_V01 base
379 editor (termed as A3A-CBE in this study), which has demonstrated efficient C-to-T
380 base editing in both rice and *Arabidopsis* under a ubiquitin promoter (Ren *et al.*,
381 2021).

382 Using this construct, we transformed Col-0 WT and *efr* mutants and assessed T1
383 progeny for T-DNA integration (via hygromycin resistance) and genome editing (via
384 tribenuron resistance conferred by *ALS* editing). The A3A-CBE system achieved an
385 overall editing frequency of approximately 0.5% in total T1 seeds and about 20%
386 among transformed individuals in the Col-0 WT background (Fig. 5b). Both *efr*-1 and
387 *efr*-2 mutants showed higher editing rates, despite the increase being statistically
388 significant only in *efr*-2. We also evaluated stable transformation efficiency by sowing
389 T1 seeds on a hygromycin-containing medium but no significant increase can be
390 observed in *efr* mutants (Fig. 5c).

391 To further validate these findings, we targeted *CLA1* and *PDS3*, two genes that
392 cause albino phenotypes when biallelically edited (Liu *et al.*, 2022). T1 seeds were
393 germinated on a hygromycin-containing medium, and the numbers of green and
394 albino seedlings were quantified (Fig. 5d). We observed a slight but consistent
395 increase in the proportion of albino seedlings in *efr*-1 compared to Col-0 WT,
396 supporting the conclusion that EFR-mediated immunity suppresses genome editing
397 efficiency during AMT-FI.

398 **Modification of *Agrobacterium* EF-Tu enhances transient gene expression and**
399 **genome editing efficiency but not stable T-DNA integration efficiency**

400 To further validate the role of EFR in suppressing genome editing efficiency during
401 AMT-FI, we tested whether an *Agrobacterium* strain that evades EFR recognition
402 mediates increased genome editing efficiency. To achieve this, we engineered
403 *Agrobacterium* to express a modified EF-Tu incapable of triggering EFR-mediated

404 PTI. *Agrobacterium* GV3101 possesses two EF-Tu-encoding genes, *tufA and tufB*,
405 which produce a translation elongation factor. Our initial attempts to delete both *tuf*
406 genes were unsuccessful, likely due to their essential function. However, a recent
407 study demonstrated that replacing the entire or N-terminal region (amino acids 1-15)
408 of *Agrobacterium* EF-Tu with that of *Pseudomonas syringae* pv. *tomato* (*Pst*)
409 DC3000 reduced PTI activation and improved transient expression efficiency in *A.*
410 *thaliana* leaves (Yang *et al.*, 2023).

411 Using a similar concept but a different experimental approach, we engineered
412 GV3101 by replacing amino acids 4-15 of both *tufA* and *tufB* with the corresponding
413 region from *Pst* EF-Tu, referred to as $tufAB^{Pst4\text{-}15}$ (Fig. 6a). We generated two
414 independent $tufAB^{Pst4\text{-}15}$ strains, named as AS201 and AS202, and compared them
415 to the parental GV3101 strain for transient expression, genome editing and stable
416 transformation efficiencies. To assess transient transformation, we transformed *A.*
417 *thaliana* seedlings for transient expression analysis using a T-DNA-encoded GUS
418 reporter (Wu *et al.*, 2014). Both AS201 and AS202 showed significantly higher
419 transient GUS activity in Col-0 WT compared to GV3101 (Fig. 6b, 6c). As expected,
420 GV3101 exhibited ~20-fold higher GUS activity in *efr*-1 than in Col-0 due to the
421 absence of EF-Tu recognition. However, in *efr*-1, AS201 and AS202 exhibited lower
422 GUS activity than GV3101, indicating that the engineered EF-Tu proteins may
423 compromise transformation efficiency when PTI is not a barrier for infection.

424 Encouraged by these results, we next tested whether the $tufAB^{Pst4\text{-}15}$ strains could
425 improve genome editing efficiencies in Col-0 by AMT-FI. Compared to GV3101, both
426 AS201 and AS202 significantly enhanced genome editing rates and produced more
427 edited T1 plants (Fig. 6d). As expected, we observed no significant difference in T-
428 DNA integration rates or in the total number of transgenic T1 plants (Fig. 6e).

429 **Sequencing-based screening of genome-edited plants**

430 Our floral inoculation analysis demonstrated that flowers opened at 6 DPI showed a
431 stable transformation efficiency ~26% (Fig. 4c). Based on this high efficiency, we
432 reasoned that it may be possible to recover genome-edited T1 plants without prior
433 selection of T-DNA integration step (Fig. 7a).

434 To test this, we targeted *CLA1* gene, which allows easy identification of edited plants
435 based on their albino phenotype, complemented by sequencing analysis. We

436 germinated T1 seeds from Col-0 and *efr* mutants on MS medium without hygromycin
437 selection. Among these seedlings, we observed biallelically edited albino plants at
438 the frequencies of 3.3% in Col-0, 3.7% in *efr*-1, and 4.2% in *efr*-2. We also identified
439 green seedings carrying monoallelic edits, identified by Sanger sequencing. Their
440 editing rates were 1.6% in Col-0, 15.9% in *efr*-1, and 4.7% in *efr*-2 (Fig. 7b). To
441 further validate this strategy, we targeted the *ALS* gene without applying tribenuron
442 selection. Among the T1 seedlings, we identified one edited plant out of 94 T1
443 seedlings using GV3101 and two out of 93 using the $tufAB^{Pst4\text{-}15}$ mutant, AS201. All
444 three edited T1 plants carried C-to-T base editing at the Pro197 locus, consistent
445 with the expected *ALS* editing outcome (Fig. 7b).

446 In conclusion, genome-edited T1 plants can be obtained without prior selection for T-
447 DNA integrated plants when screening seeds from flowers opened at 6 DPI.
448 Furthermore, evading EFR-mediated PTI enhances genome editing efficiency,
449 further supporting the role of plant immunity in constraining *Agrobacterium*-based
450 genome engineering.

451

452 **DISCUSSION**

453 In this study, we provide mechanistic and practical insights into the *Agrobacterium*-
454 mediated floral transformation process. By tracking transformation events with a
455 dual-reporter system, we identified the optimal transformation window, leading to the
456 success in obtaining edited plants without prior selection of T-DNA integration. Our
457 findings also reveal EFR-mediated immunity as a key barrier to efficient transient
458 transformation and genome editing via AMT-FI. By integrating floral stage selection,
459 immune evasion, and *Agrobacterium* engineering, this study provides a versatile
460 platform to advance plant genome engineering.

461 **Different cell types exhibit varying susceptibility to *Agrobacterium* infection**

462 Using RUBY as a T-DNA reporter, we detected strong RUBY signals in sepal,
463 transmitting tissues, ovules, and developing seeds (Fig. 2). Notably, no RUBY
464 signals were detected in pollen grains, consistent with earlier findings using GUS
465 reporter (Ye *et al.*, 1999; Bechtold *et al.*, 2000; Desfeux *et al.*, 2000). The variation in
466 transformation efficiency likely reflects cell-type specific susceptibility to

467 *Agrobacterium* infection or differential transcriptional activity of the CaMV 35S
468 promoter (Kiselev *et al.*, 2021). Additionally, we observed diverse RUBY expression
469 patterns among hygromycin-resistant transgenic plants. Some plants expressed
470 RUBY throughout their life cycle, while others showed expression only during
471 seedling stages or specific organs. This variability may result from positional effects
472 of T-DNA integration site or differences in promoter activity (Gelvin, 2003; Roca
473 Paixao & Deleris, 2024). The presence of hygromycin-sensitive but RUBY-positive
474 seedlings also suggests a possible truncation of the T-DNA at the left border (Fig.
475 3a), where the hygromycin resistance cassette is located.

476 **Temporal and spatial tracking of *Agrobacterium* entry and transformation**

477 Although various floral tissues and cell types can be transformed (Fig. 1, 2), only
478 female gametes serve as heritable targets for producing progenies in *Arabidopsis*
479 (Ye *et al.*, 1999; Bechtold *et al.*, 2000; Desfeux *et al.*, 2000). Therefore,
480 *Agrobacterium* entry into the locule of developing gynoecium is a crucial step in
481 successful transformation (Desfeux *et al.*, 2000).

482 Our data show that *Agrobacterium* enters the locule of open gynoecium within hours,
483 colonizes reproductive tissues, and persists around the micropyle of ovules,
484 potentially enabling transformation of egg cells and surrounding tissues. Despite
485 early colonization, transformation events in gynoecium cells only occur in open
486 flowers from 5 DPI onward, coinciding with floral opening and micropyle exposure.

487 Transient T-DNA expression can be observed as early as 1 DPI and highly abundant
488 at 2 DPI when transforming somatic cells like leaves, seedlings, and root explants
489 (Gelvin, 2003; Wu *et al.*, 2014; Lopez-Agudelo *et al.*, 2024). The delayed expression
490 in germ cells may reflect differences in promoter activity, cell-type susceptibility, or
491 route of *Agrobacterium* entry. Given that pollen tubes access ovules via the
492 micropyle only after floral opening, they may serve as important carriers, facilitating
493 *Agrobacterium* entry into ovules for transformation. Once inside, *Agrobacterium*
494 could associate with male gametes or directly attach to egg cells for T-DNA transfer
495 during fertilization. This proposed mechanism explains the high AMT-FI efficiency
496 observed in flowers opening at 5-9 DPI and suggests that transformation occurs in
497 young floral buds 5-9 days before anthesis, supporting previous findings (Clough &
498 Bent, 1998; Ye *et al.*, 1999; Desfeux *et al.*, 2000).

499 **AMT peaks in flowers opened at 6 DPI and negatively correlate with seed**
500 **viability**

501 Tracking transformation events by fluorescent marker revealed *Agrobacterium*
502 targets integument cells (Fig. 1l, 1m), consistent with previous findings (Bechtold *et*
503 *al.*, 2003). However, only the transformed egg cells contribute to transgene
504 inheritance. This explains why RUBY-based transformation rates are significantly
505 higher than those determined by hygromycin resistance (Fig. 3c, 4c). The use of the
506 RUBY reporter enabled the discovery of floral stages accessible for AMT-FI,
507 revealing that nearly all ovaries from flowers open at 6 DPI were transformed (Fig.
508 4b), yielding averaged an 26% stable Hyg^R T1 progeny. However, high
509 transformation rates were accompanied by increased ovule abortion, resulting in
510 fewer viable seeds (Figs. 3d, 4c, 4a). In contrast, *efr* mutants exhibited lower
511 abortion rates and higher seed viability per silique, suggesting that EFR-triggered
512 immunity contributes to transformation-induced ovule loss. Evading plant immune
513 responses could therefore enhance the efficiency of transgenic seed production via
514 AMT-FI.

515 **Evasion of EFR-mediated immunity enhances genome editing efficiency but**
516 **not stable transformation**

517 Although EFR-mediated immunity was discovered nearly two decades ago (Zipfel *et*
518 *al.*, 2006), its influence on stable transformation and genome editing remain unclear.
519 While *efr*-1 mutants showed no improvement on gene targeting or stable
520 transformation efficiencies (van Tol *et al.*, 2022), they do exhibit enhanced transient
521 expression (Zipfel et al., 2006; Wu, Liu et al., 2014; Yang et al., 2023). Our results
522 confirm higher RUBY transformation rates in *efr* ovules, but no significant increase in
523 stable transformation measured by hygromycin resistance (Figs. 4c, 6e).

524 However, we showed that genome editing efficiencies were significantly higher in *efr*
525 mutants and in Col-0 WT inoculated with the two engineered GV3101::$tufAB^{Pst4\text{-}15}$
526 strain, AS201 and AS202 (Figs. 5, 6). This suggests that genome editing can be
527 decoupled from T-DNA integration. This is further supported by evidence that
528 genome-edited plants were successfully obtained from the *teb-5* (*polQ)* mutant,
529 whereas T-DNA integrated plants were not (van Tol *et al.*, 2022). Thus, we proposed
530 that enhancement of editing efficiencies may result from higher transient expression

531 of CRISPR/Cas9 in egg cells in the absence of EFR-triggered immunity. Moreover,
532 because editing can occur without DNA integration (e.g., via ribonucleoprotein
533 delivery), it may serve as a proxy for measuring transgene expression levels in
534 germline cells.

535 **Innovative strategies for enhancing genome editing efficiency**

536 Precision editing is critical for inducing dominant phenotypes by targeting an
537 endogenous gene. However, current methods exhibit low efficiency compared to
538 mutagenesis by Cas9 nuclease (Huang & Puchta, 2021). To overcome these
539 limitations, we used an improved A3A-CBE base editor and achieved a high editing-
540 to-integration ratio (~0.2) (Fig. 5). This construct, together with our optimized
541 screening workflow, enables efficient dissection factors that influence stable
542 transformation and genome editing efficiency in *Arabidopsis*.

543 Several recent studies have introduced innovative approaches to enhance stable
544 transformation and genome editing. These include engineering of *Agrobacterium*
545 strains to deliver type III secretion system effectors, T-DNA concatenation, and
546 vector copy number manipulation (Raman *et al.*, 2022; Dickinson *et al.*, 2023;
547 Szarzanowicz *et al.*, 2024). Our success in engineering *Agrobacterium* strains with
548 modified EF-Tu to evade EFR recognition, significantly enhanced genome editing
549 efficiency. This reinforces the idea that boosting transient gene expression is a key
550 determinant for successful genome modification via CRISPR/Cas9.

551 Despite native EFR is specific to Brassicaceae, several non-Brassicaceae crops
552 have been engineered to express EFR for disease resistance (Lu *et al.*, 2015;
553 Schwessinger *et al.*, 2015; Boschi *et al.*, 2017; Kunwar *et al.*, 2018; Piazza *et al.*,
554 2021). These transgenic plants may show reduced *Agrobacterium*-mediated
555 transformation. Our engineered GV3101::*tufAB*$^{Pst4\text{-}15}$ strains could overcome this
556 limitation. Beyond EF-Tu, other *Agrobacterium*-derived PAMPs such as translation
557 initiation factor IF1, cold-shock protein, and flagellin also trigger PTI via distinct
558 receptors in different species (Saur *et al.*, 2016; Fürst *et al.*, 2020; Fan *et al.*, 2022).
559 This work sets the stage for the development of multi-modified *Agrobacterium* strains
560 with broad compatibility, offering a roadmap to enhance AMT across diverse plant
561 taxa.

562

AUTHOR CONTRIBUTIONS

M.-S.L, T.-K.H., C.-H. K. and E.-M.L, contributed to the conceptualization of the project. M.-S.L. designed and performed AMT-FI. T.-K.H. designed and performed the genome editing assay. M.-S.L., T.-K.H., Y.-C.W. and S.-C.W. performed experiments and analyzed data. M.-S.L., T.-K.H., and E.-M.L. wrote the initial manuscript. E.-M.L., C.-H. K. and C.-H.W. supervised the project. All authors reviewed and edited the manuscript.

ACKNOWLEDGEMENTS

The authors acknowledge the members of the Lai, Kuo, and Wu labs for discussion and suggestion. We also thank the technical assistance of Live Cell Imaging Core Lab and Sanger DNA sequencing service provided by Genomic Technology Core located at the Institute of Plant and Microbial Biology, Academia Sinica. The funding was supported by the Academia Sinica Grand Challenge Program (AS-GC-111-L02) to E.-M.L., C.-H. K. and C.-H.W, and the intramural fund of the Institute of Plant and Microbial Biology, Academia Sinica.

SUPPORTING INFORMATION

Table S1. Plasmid information

Table S2. Primer list

Figures S1-S5

CONFLICT OF INTEREST STATEMENT

The authors declare no conflict of interest.

588 **FIGURE LEGENDS**

589

590 **Figure 1. *Agrobacterium* enter open gynoecium within 1 hour but**
591 **transformation events occur in open flowers after 5 days post inoculation**

592 *Agrobacterium* GV3101 carrying pRL662-GFP(S65T)/Spe^R and the binary vector
593 35S::mCherry2-NLS was used for floral inoculation on *Arabidopsis thaliana* Col-0 to
594 visualize *Agrobacterium* localization and transformation events (a). Schematic
595 illustration of the structure and development of gynoecium from early to mature stage
596 with stigma, style, ovary containing ovules (b). The floral stages and their
597 corresponding durations were indicated according to Smyth et al. (Smyth et al.,
598 1990)

599 After one hour post-inoculation (HPI), *Agrobacterium* cells had already entered the
600 locule of developing gynoecium (c) but were absent in later-stage gynoecia
601 containing developed placenta tissue (d). Between 6-9 HPI, more *Agrobacterium*
602 cells were observed in the locule (e), even at it began to close (f). *Agrobacterium*
603 was not detected in fully closed gynoecia (g).

604 At one day post-inoculation (DPI), *Agrobacterium* cells were detected in young
605 closed ovaries (h) but not in older ovaries undergoing ovule development (i). At 3
606 DPI (j), *Agrobacterium* cells persisted in ovaries at late developmental stages. By 5
607 DPI, *Agrobacterium* cells were enriched around the micropyle (arrow) (k), though no
608 mCherry2 signal was detected. At floral open stage after 6 DPI, *Agrobacterium*
609 accumulated around the micropyle, and mCherry2 signal became visible (l and m).

610 Asterisks (*) indicate placenta tissue; arrowheads denote developing ovule; arrows
611 indicate *Agrobacterium* located around micropyle. Panels (a to k) were merged
612 channel images; panels (l and m) show GFP, mCherry2, DIC and merged views.
613 Scale bar= 100 μm.

614 **Figure 2. RUBY marker revealed transformation events in floral organs and**
615 **female tissues**

616 RUBY signals were observed in flowers (a), specifically on the stigma but not on
617 pollen grains (b), and in the transmitting tissue (c). In siliques, RUBY expression was
618 detected in both abortive (d) and developing ovules (e).

619 Flower morphology after AMT-FI ranged from normal open flowers (f) to partially
620 open flowers (g), and flowers with only gynoecia emerging from sepals (h), all with
621 visible RUBY signals.

622 RUBY signal intensity varied among seeds (i) and plants (j, k). (j) At the seedling
623 stage, hygromycin resistant (Hyg^R) and RUBY-positive seedling (left), non-transgenic
624 seedling (middle), and RUBY-positive but hygromycin sensitive (Hyg^S) seedling
625 (right) were observed. (k) Transgenic T1 plants with variable RUBY expression
626 patterns from strong whole-plant expression to undetectable signal. Scale bar = 200
627 μm.

628 **Figure 3. *Agrobacterium* infection and EFR-mediated immunity exert negative**
629 **impacts on ovule development**

630 (a) Experimental design: a schematic diagram illustrates the 35S::RUBY construct
631 and experimental workflow. Transformation efficiency was evaluated based on the
632 presence of RUBY-positive ovules and hygromycin-resistant seedlings.

633 (b) Percentage of siliques with RUBY-positive ovules recorded daily for Col-0 WT,
634 *efr*-1, and *efr*-2 from flowers that opened at 1-10 DPI. Data are mean ± SD of three
635 biological replicates from representative of two independent experiments.

636 (c) RUBY-based transformation. Percentage of RUBY-positive ovules (include both
637 developed and abortive ovules) per silique collected from flowers of Col-0 WT, *efr*-1
638 and *efr*-2 opened at 5-9 DPI was calculated (all data points shown in Fig. S2a). Data
639 are mean ± SD of averaged percentage of RUBY-positive ovules from three
640 independent experiments (circle, triangle and rhombus symbols). Statistically
641 significant differences ($p < 0.05$) between Col-0 WT and *efr* mutants are indicated.

642 (d) Ovule abortion rate. The abortion rate of RUBY-positive, non-RUBY, and total
643 ovules per silique collected from flowers of Col-0 WT, *efr*-1 and *efr*-2 opened at 5-9
644 DPI was calculated (all data points shown in Fig. S2c). Data are mean ± SD of
645 averaged abortion rate from three independent experiments (circle, triangle and
646 rhombus symbols). Statistically significant differences ($p < 0.05$) between Col-0 WT
647 and *efr* mutants are indicated.

648 **Figure 4. AMT events occur mainly in flowers opened at 5-9 DPI, peaking at 6**
649 **DPI**

650 Siliques and seeds developed from flowers that opened at 5-9 DPI in Col-0 WT, *efr*-1
651 and *efr*-2 mutants were analyzed through viability (a) and hygromycin resistance
652 (Hyg^R) screening (b, c, d) and viability (d). Data are (a) number of viable seeds per
653 silique, (b) percentage of siliques containing Hyg^R transformants, (c) percentage of
654 Hyg^R transformants per silique and (d) number of Hyg^R transformants per plant. Data
655 are mean ± SD of six biological replicates from two independent experiments (circle
656 and triangle symbols). Statistically significant differences ($p < 0.05$) between Col-0
657 WT and *efr* mutants are indicated.

658 **Figure 5. EFR suppresses genome editing efficiency**

659 *Agrobacterium* GV3101 carrying a binary vector encoding a base editor and a
660 sgRNA was used for floral inoculation in Col-0 WT and *efr* mutants to assess
661 genome editing and stable transformation efficiencies. (a) A schematic diagram of
662 the binary vector structure for base editing and target gene information. (b) Genome
663 editing efficiency assessed by tribenuron resistant T1 plants with targeting the *ALS*
664 Pro197 locus. (c) Stable transformation efficiency evaluated by hygromycin
665 resistance. Seeds are collected from flowers that opened at 5-9 DPI. Data are mean
666 ± SD, with *p*-values calculated by Student's t-test between Col-0 WT and *efr*
667 mutants. (d) Genome editing efficiency assessed based on albino phenotype in T1
668 plants, resulting from by loss-of-function mutations at locus *CLA1 and PDS3.*
669 Statistically significant differences between Col-0 WT and *efr* are indicated (*$p <$
670 0.05, **$p < 0.01$, chi-square analysis).

671 **Figure 6. Modification of *Agrobacterium* EF-Tu enhances transient gene**
672 **expression and genome editing efficiency but not stable T-DNA integration**
673 **efficiency**

674 The two engineered *Agrobacterium tufAB*$^{Pst4\text{-}15}$ strains, AS201 and AS202, were
675 assessed for its efficiency in transient expression, genome editing, and stable
676 transformation in comparison to the parental *Agrobacterium* GV3101.

677 (a) A schematic diagram illustrating the difference of *tufAB* sequences at amino
678 acids 4th to 15th between *Agrobacterium* GV3101 and *Pseudomonas syringae* (*Pst*).

679 (b, c) Comparison of transient transformation efficiencies between the GV3101 WT
680 and two *tufAB*$^{Pst4\text{-}15}$ strains (AS201 and AS202) in *A. thaliana* seedlings by

681 quantitative GUS activity (b) GUS staining (c, scale bar =1 cm). Results are
682 representative of three independent experiments.

683 (d) Comparison of genome editing efficiency between the GV3101 WT and two
684 *tufAB*$^{Pst4\text{-}15}$ strains (AS201 and AS202) measured by the percentage of tribenuron-
685 resistant T1 plants (left) and number of edited T1 plants per three T0 plants (right).

686 (e) Comparison of stable transformation efficiency by the number of hygromycin-
687 resistant T1 plants per three T0 plants, with no significant differences between WT
688 GV3101 and the two *tufAB*$^{Pst4\text{-}15}$ strains (AS201 and AS202).

689 Seeds were collected from all flowers. Each data point represents biological
690 replicates from three independent experiments. All values are shown as mean ± SD,
691 with *p*-values calculated by Student's t-test.

692 **Figure 7. Sequencing-based screening of genome-edited plants**

693 (a) Workflow for screening genome-edited T1 plants from flowers that opened at 6
694 DPI. Seeds were germinated in 1/2 MS medium with only supplemented with
695 timentin to suppress *Agrobacterium* growth without hygromycin selection. 10-day-old
696 T1 plants were analyzed by Sanger sequencing at the *ALS* or *CLA1* loci.

697 (b) The number of sequenced T1 plants and editing rates. †indicates the C to T
698 editing at Pro197 locus conferring tribenuron resistance. Statistically significant
699 differences in genome editing (GE) rates between *efr*-1 and WT Col-0 are indicated
700 (*$p < 0.001$, chi-square analysis).

701 **Figure S1. Basipetal analysis of *Agrobacterium* distribution along Arabidopsis**
702 **inflorescence at 1 DPI.**

703 A basipetal series of flowers from the inflorescence tip (a) to the first open flower at
704 the base (m and n) were dissected to visualize Agrobacterium expressing GFP
705 reporter at 1 DPI. Figures (m) and (n) are from different regions of the same flower.
706 Each figure consists of four imaging channels (o). Scale bars indicated 50 μm.

707 **Figure S2. Number and percentage of Hyg^{R}/RUBY^{+} T1 seedlings.**

708 (a) Representative photo of T1 seedlings screening on hygromycin containing 1/2
709 MS plate. The hygromycin-resistant T1 exhibiting RYBY signals of whole seedling
710 (Hyg^{R}/RUBY^{+}) was indicated, among the hygromycin-resistant green and larger T1

711 seedling (Hyg^R/$RUBY^-$), and hygromycin-sensitive green but small seedlings
712 (Hyg^S/$RUBY^-$). The hygromycin-sensitive T1 seedlings with RUBY signals
713 (Hyg^S/$RUBY^+$) shown in Fig. 2j are rarely occurred and not present in this photo.

714 (b) Number and percentage of Hyg^R/$RUBY^+$ T1 seedlings in Col-0 WT and *efr*
715 mutants. Total number of Hyg^R T1 seedlings (Total) and those exhibiting RYBY
716 signals of whole seedling ($RUBY^+$) was indicated and the percentage of Hyg^R/$RUBY^+$
717 T1s among total Hyg^R T1s.

718 **Figure S3. EFR-mediated immunity exerts negative impacts on ovule**
719 **development and RUBY-based transformation rate**

720 GV3101 carrying the 35S::RUBY construct was used for AMT-FI to assess RUBY-
721 based transformation efficiency and ovule abortion rate in Col-0 WT and *efr* mutants.
722 Siliques from flowers that opened at 5-9 DPI were analyzed to count the total
723 number of ovules, the number of developed ovules with or without RUBY signals,
724 and the number of abortive ovules with or without RUBY signals per silique.

725 (a) Daily RUBY-based transformation rate per silique. The percentage of RUBY-
726 positive ovules (including both developed and abortive ovules) per silique was
727 calculate at each DPI, as well as cumulatively across 5-9 DPI. Each data point
728 represents the percentage of RUBY-positive ovules per silique.

729 (b) Daily RUBY-based transformation rate of developed ovules per silique. The
730 percentage of RUBY-positive developed (non-abortive) ovules per silique was
731 measured at each DPI, as well as cumulatively across 5-9 DPIs. Each data point
732 represents the percentage of RUBY-positive developed ovules per silique.

733 (c) Daily ovule abortion rate per silique. The percentage of abortive ovules (including
734 both RUBY-positive and RUBY-negative) per silique was recorded at each DPI and
735 cumulatively across 5-9 DPI. Each data point represents the percentage of abortive
736 ovules per silique.

737 Data are shown in mean ± SD from three independent experiments, with *p*-values
738 calculated by Student's t-test between Col-0 WT and *efr* mutants.

739 Related to Figure 3.

740 **Figure S4. Silique and seed number in Col-0 WT, *efr*-1 and *efr*-2 mutants after**
741 **AMT-FI.**

742 Number of siliques (a) and seeds (b) developed from flowers that opened at 5-9 DPI
743 per plant in Col-0 WT, *efr*-1 and *efr*-2 mutants were analyzed. Data are mean ± SD
744 of six biological replicates from two independent experiments (circle and triangle
745 symbols).

746 **Figure S5. *Agrobacterium* infection and EFR-mediated immunity affect seed**
747 **outputs**

748 (a) Table showing seed number per silique from plants treated with infiltration
749 medium alone or with *Agrobacterium.* Percentages of developed and germinated
750 seeds after *Agrobacterium* infection, indicating the impact on seed viability. (b) Seed
751 counts and germination rates following infiltration medium alone (IM) or with
752 *Agrobacterium* IM (IM + GV3101) treatments. Siliques were collected from flowers
753 that opened at 5–9 DPI. The total number of seeds and the number of germinated
754 seeds were compared between treatments. Data were collected from two plants per
755 genotype, except for *efr*-1 infected with GV3101, where data were obtained from one
756 plant. Data are shown as mean ± SD, with *p*-values calculated using Student's *t*-test
757 to compare Col-0 WT and *efr* mutants.

758

759

REFERENCES

Anand A, Uppalapati SR, Ryu CM, Allen SN, Kang L, Tang Y, Mysore KS. 2008. Salicylic acid and systemic acquired resistance play a role in attenuating crown gall disease caused by *Agrobacterium tumefaciens*. *Plant Physiol.* **146**(2): 703-715.

Angulo J, Astin CP, Bauer O, Blash KJ, Bowen NM, Chukwudinma NJ, DiNofrio AS, Faletti DO, Ghulam AM, Gusinde-Duffy CM, et al. 2023. CRISPR/Cas9 mutagenesis of the *Arabidopsis* GROWTH-REGULATING FACTOR (GRF) gene family. *Front. Genome Ed.* **5**: 1251557.

Baud S, Boutin J-P, Miquel M, Lepiniec L, Rochat C. 2002. An integrated overview of seed development in *Arabidopsis thaliana* ecotype WS. *Plant Physiol. Biochem.* **40**(2): 151-160.

Bechtold N, Jaudeau B, Jolivet S, Maba B, Vezon D, Voisin R, Pelletier G. 2000. The maternal chromosome set is the target of the T-DNA in the in planta transformation of *Arabidopsis thaliana*. *Genetics* **155**(4): 1875-1887.

Bechtold N, Jolivet S, Voisin R, Pelletier G. 2003. The endosperm and the embryo of *Arabidopsis thaliana* are independently transformed through infiltration by *Agrobacterium tumefaciens*. *Transgenic Res.* **12**(4): 509-517.

Bélanger JG, Copley TR, Hoyos-Villegas V, Charron JB, O'Donoughue L. 2024. A comprehensive review of in planta stable transformation strategies. *Plant Methods* **20**(1): 79.

Bevan M. 1984. Binary *Agrobacterium* vectors for plant transformation. *Nucleic Acids Res.* **12**(22): 8711-8721.

Boschi F, Schvartzman C, Murchio S, Ferreira V, Siri MI, Galván GA, Smoker M, Stransfeld L, Zipfel C, Vilaró FL, et al. 2017. Enhanced bacterial wilt resistance in potato through expression of *Arabidopsis* EFR and introgression of quantitative resistance from *Solanum commersonii*. *Front. Plant Sci.* **8**: 1642.

Chen Y, Wang Z, Ni H, Xu Y, Chen Q, Jiang L. 2017. CRISPR/Cas9-mediated base-editing system efficiently generates gain-of-function mutations in *Arabidopsis*. *Sci. China Life Sci.* **60**(5): 520-523.

Clough SJ, Bent AF. 1998. Floral dip: a simplified method for *Agrobacterium*-mediated transformation of *Arabidopsis thaliana*. *Plant J.* **16**(6): 735-743.

Desfeux C, Clough SJ, Bent AF. 2000. Female reproductive tissues are the primary target of *Agrobacterium*-mediated transformation by the *Arabidopsis* floral-dip method. *Plant Physiol.* **123**(3): 895-904.

Dickinson L, Yuan W, LeBlanc C, Thomson G, Wang S, Jacob Y. 2023. Regulation of gene editing using T-DNA concatenation. *Nat. Plants* **9**(9): 1398-1408.

Dodds PN, Chen J, Outram MA. 2024. Pathogen perception and signaling in plant immunity. *Plant Cell* **36**(5): 1465-1481.

Fan L, Fröhlich K, Melzer E, Pruitt RN, Albert I, Zhang L, Joe A, Hua C, Song Y, Albert M, et al. 2022. Genotyping-by-sequencing-based identification of *Arabidopsis* pattern recognition receptor RLP32 recognizing proteobacterial translation initiation factor IF1. *Nat. Commun.* **13**(1): 1294.

Fürst U, Zeng Y, Albert M, Witte AK, Fliegmann J, Felix G. 2020. Perception of *Agrobacterium tumefaciens* flagellin by FLS2(XL) confers resistance to crown gall disease. *Nat. Plants* **6**(1): 22-27.

Gelvin SB. 2003. *Agrobacterium*-mediated plant transformation: the biology behind the "gene-jockeying" tool. *Microbiol. Mol. Biol. Rev.* **67**(1): 16-37, table of contents.

Hooykaas PJJ. 2023. The Ti plasmid, driver of *Agrobacterium* pathogenesis. *Phytopathology* **113**(4): 594-604.

Huang T-K, Puchta H. 2021. Novel CRISPR/Cas applications in plants: from prime editing to chromosome engineering. *Transgenic Res.* **30**(4): 529-549.

Hwang HH, Yu M, Lai EM. 2017. *Agrobacterium*-mediated plant transformation: biology and applications. *Arabidopsis Book* **15**: e0186.

810 **Kado CI, Heskett MG. 1970.** Selective media for isolation of *Agrobacterium*, *Corynebacterium*,
811 *Erwinia*, *Pseudomonas*, and *Xanthomonas*. *Phytopathology* **60**(6): 969-976.
812 **Kiselev KV, Aleynova OA, Ogneva ZV, Suprun AR, Dubrovina AS. 2021.** 35S promoter-driven
813 transgenes are variably expressed in different organs of *Arabidopsis thaliana* and in
814 response to abiotic stress. *Mol. Biol. Rep.* **48**(3): 2235-2241.
815 **Kunwar S, Iriarte F, Fan Q, Evaristo da Silva E, Ritchie L, Nguyen NS, Freeman JH, Stall RE, Jones JB,**
816 **Minsavage GV, et al. 2018.** Transgenic expression of EFR and Bs2 genes for field
817 management of bacterial wilt and bacterial spot of Tomato. *Phytopathology* **108**(12): 1402-
818 1411.
819 **Lacroix B, Citovsky V. 2019.** Pathways of DNA transfer to plants from *Agrobacterium tumefaciens*
820 and related bacterial species. *Annu. Rev. Phytopathol.* **57**: 231-251.
821 **Liu D, Xuan S, Prichard LE, Donahue LI, Pan C, Nagalakshmi U, Ellison EE, Starker CG, Dinesh-Kumar**
822 **SP, Qi Y, et al. 2022.** Heritable base-editing in *Arabidopsis* using RNA viral vectors. *Plant*
823 *Physiol.* **189**(4): 1920-1924.
824 **Lopez-Agudelo JC, Goh F-J, Tchabashvili S, Huang Y-S, Huang C-Y, Lee K-T, Wang Y-C, Wu Y, Chang**
825 **H-X, Kuo C-H, et al. 2024.** *Rhizobium rhizogenes* A4-derived strains mediate hyper-efficient
826 transient gene expression in *Nicotiana benthamiana* and other solanaceous plants. *Plant*
827 *Biotechnol. J.*
828 **Lu F, Wang H, Wang S, Jiang W, Shan C, Li B, Yang J, Zhang S, Sun W. 2015.** Enhancement of innate
829 immune system in monocot rice by transferring the dicotyledonous elongation factor Tu
830 receptor EFR. *J. Integr. Plant Biol.* **57**(7): 641-652.
831 **Mysore KS, Kumar CT, Gelvin SB. 2000.** *Arabidopsis* ecotypes and mutants that are recalcitrant to
832 *Agrobacterium* root transformation are susceptible to germ-line transformation. *Plant J.*
833 **21**(1): 9-16.
834 **Nam J, Matthysse AG, Gelvin SB. 1997.** Differences in susceptibility of *Arabidopsis* ecotypes to
835 crown gall disease may result from a deficiency in T-DNA integration. *Plant Cell* **9**(3): 317-
836 333.
837 **Nishizawa-Yokoi A, Saika H, Hara N, Lee LY, Toki S, Gelvin SB. 2021.** *Agrobacterium* T-DNA
838 integration in somatic cells does not require the activity of DNA polymerase θ. *New Phytol.*
839 **229**(5): 2859-2872.
840 **Piazza S, Campa M, Pompili V, Costa LD, Salvagnin U, Nekrasov V, Zipfel C, Malnoy M. 2021.** The
841 *Arabidopsis* pattern recognition receptor EFR enhances fire blight resistance in apple. *Hortic.*
842 *Res.* **8**.
843 **Pixley KV, Falck-Zepeda JB, Paarlberg RL, Phillips PWB, Slamet-Loedin IH, Dhugga KS, Campos H,**
844 **Gutterson N. 2022.** Genome-edited crops for improved food security of smallholder farmers.
845 *Nat. Genet.* **54**(4): 364-367.
846 **Raman V, Rojas CM, Vasudevan B, Dunning K, Kolape J, Oh S, Yun J, Yang L, Li G, Pant BD, et al.**
847 **2022.** *Agrobacterium* expressing a type III secretion system delivers *Pseudomonas* effectors
848 into plant cells to enhance transformation. *Nat. Commun.* **13**(1): 2581.
849 **Ren Q, Sretenovic S, Liu G, Zhong Z, Wang J, Huang L, Tang X, Guo Y, Liu L, Wu Y, et al. 2021.**
850 Improved plant cytosine base editors with high editing activity, purity, and specificity. *Plant*
851 *Biotechnol. J.* **19**(10): 2052-2068.
852 **Roca Paixao JF, Deleris A. 2024.** Epigenetic control of T-DNA during transgenesis and pathogenesis.
853 *Plant Physiol.* **197**(1).
854 **Saur IM, Kadota Y, Sklenar J, Holton NJ, Smakowska E, Belkhadir Y, Zipfel C, Rathjen JP. 2016.**
855 NbCSPR underlies age-dependent immune responses to bacterial cold shock protein in
856 *Nicotiana benthamiana*. *Proc. Natl. Acad. Sci. U. S. A.* **113**(12): 3389-3394.
857 **Schwessinger B, Bahar O, Thomas N, Holton N, Nekrasov V, Ruan D, Canlas PE, Daudi A, Petzold CJ,**
858 **Singan VR, et al. 2015.** Transgenic expression of the dicotyledonous pattern recognition
859 receptor EFR in rice leads to ligand-dependent activation of defense responses. *PLoS Pathog.*
860 **11**(3): e1004809.

Shih PY, Chou SJ, Müller C, Halkier BA, Deeken R, Lai EM. 2018. Differential roles of glucosinolates and camalexin at different stages of *Agrobacterium*-mediated transformation. *Mol. Plant Pathol.* **19**(8): 1956-1970.

Smyth DR, Bowman JL, Meyerowitz EM. 1990. Early flower development in Arabidopsis. *Plant Cell* **2**(8): 755-767.

Steinert J, Schiml S, Fauser F, Puchta H. 2015. Highly efficient heritable plant genome engineering using Cas9 orthologues from *Streptococcus thermophilus* and *Staphylococcus aureus*. *Plant J.* **84**(6): 1295-1305.

Suzuki K, Tanaka K, Yamamoto S, Kiyokawa K, Moriguchi K, Yoshida K 2009. Ti and Ri plasmids. In: Schwartz E ed. *Microbial Megaplasmids*. Berlin, Heidelberg: Springer Berlin Heidelberg, 133-147.

Szarzanowicz MJ, Waldburger LM, Busche M, Geiselman GM, Kirkpatrick LD, Kehl AJ, Tahmin C, Kuo RC, McCauley J, Pannu H, et al. 2024. Binary vector copy number engineering improves *Agrobacterium*-mediated transformation. *Nat. Biotechnol.*

Tiwari M, Mishra AK, Chakrabarty D. 2022. *Agrobacterium*-mediated gene transfer: recent advancements and layered immunity in plants. *Planta* **256**(2): 37.

van Kregten M, de Pater S, Romeijn R, van Schendel R, Hooykaas PJ, Tijsterman M. 2016. T-DNA integration in plants results from polymerase-θ-mediated DNA repair. *Nat. Plants* **2**(11): 16164.

van Tol N, van Schendel R, Bos A, van Kregten M, de Pater S, Hooykaas PJJ, Tijsterman M. 2022. Gene targeting in polymerase theta-deficient *Arabidopsis thaliana*. *Plant J.* **109**(1): 112-125.

Wang Y-C, Yu M, Shih P-Y, Wu H-Y, Lai E-M. 2018. Stable pH suppresses defense signaling and is the key to enhance *Agrobacterium*-mediated transient expression in *Arabidopsis* seedlings. *Sci. Rep.* **8**(1): 17071.

Wang Z-P, Xing H-L, Dong L, Zhang H-Y, Han C-Y, Wang X-C, Chen Q-J. 2015. Egg cell-specific promoter-controlled CRISPR/Cas9 efficiently generates homozygous mutants for multiple target genes in *Arabidopsis* in a single generation. *Genome Biol.* **16**(1): 144.

Weisberg AJ, Wu Y, Chang JH, Lai EM, Kuo CH. 2023. Virulence and Ecology of Agrobacteria in the Context of Evolutionary Genomics. *Annu. Rev. Phytopathol.* **61**: 1-23.

Wu H-Y, Liu K-H, Wang Y-C, Wu J-F, Chiu W-L, Chen C-Y, Wu S-H, Sheen J, Lai E-M. 2014. AGROBEST: an efficient *Agrobacterium*-mediated transient expression method for versatile gene function analyses in *Arabidopsis* seedlings. *Plant Methods* **10**(1): 19.

Yang F, Li G, Felix G, Albert M, Guo M. 2023. Engineered *Agrobacterium* improves transformation by mitigating plant immunity detection. *New Phytol.* **237**(6): 2493-2504.

Ye GN, Stone D, Pang SZ, Creely W, Gonzalez K, Hinchee M. 1999. *Arabidopsis* ovule is the target for *Agrobacterium* in planta vacuum infiltration transformation. *Plant J.* **19**(3): 249-257.

Yu M, Wang YC, Huang CJ, Ma LS, Lai EM. 2021. *Agrobacterium tumefaciens* deploys a versatile antibacterial strategy to increase its competitiveness. *J. Bacteriol.* **203**(3): e00490-00420.

Zipfel C, Kunze G, Chinchilla D, Caniard A, Jones JDG, Boller T, Felix G. 2006. Perception of the bacterial PAMP EF-Tu by the receptor EFR restricts *Agrobacterium*-mediated transformation. *Cell* **125**(4): 749-760.

Figure 1

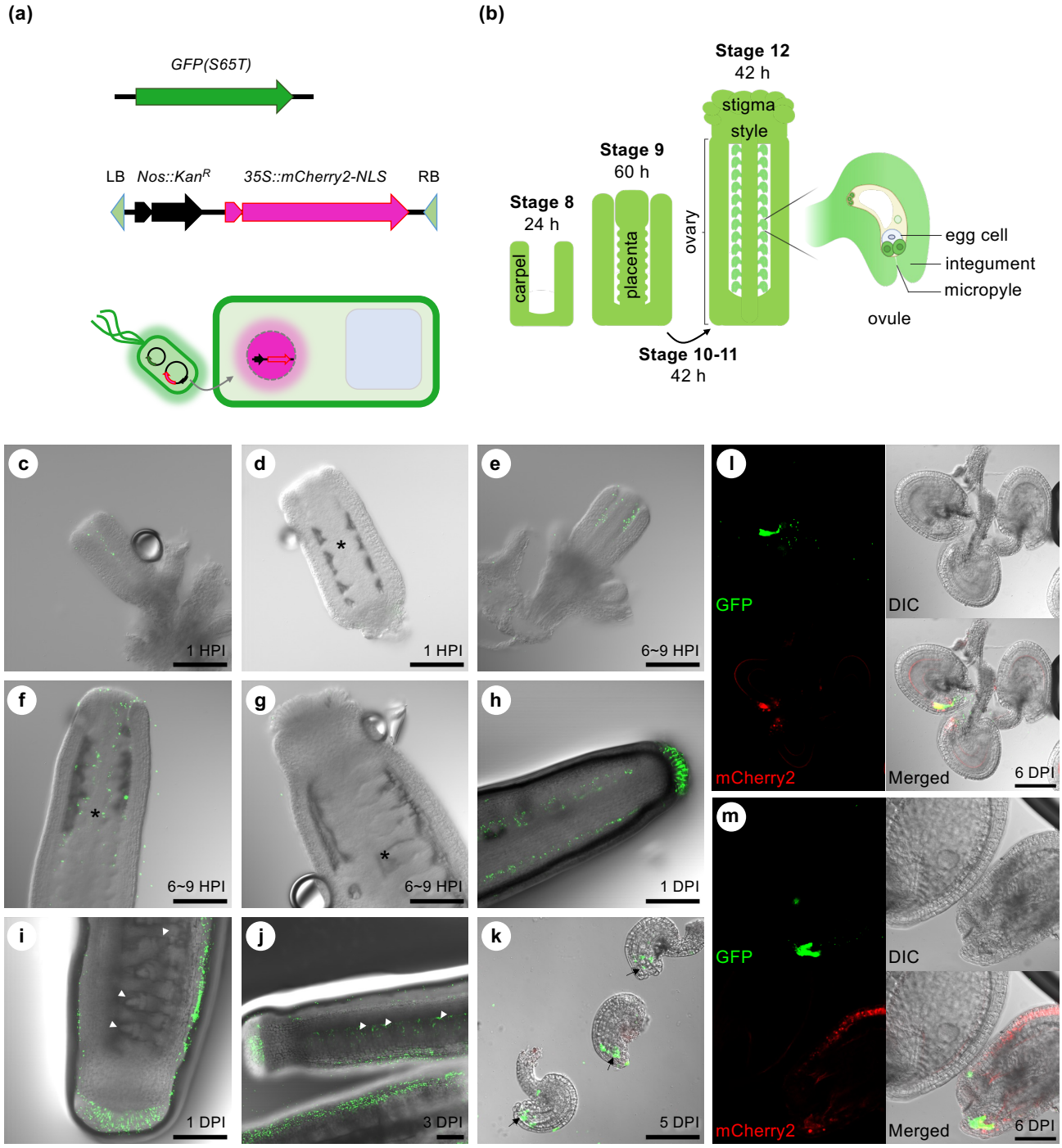

Figure 1. *Agrobacterium* enter open gynoecium within 1 hour but transformation events occur in open flowers after 5 days post inoculation

Agrobacterium GV3101 carrying pRL662-GFP(S65T)/Spe^R and the binary vector 35S::mCherry2-NLS was used for floral inoculation on *Arabidopsis thaliana* Col-0 to visualize *Agrobacterium* localization and transformation events (a). Schematic illustration of the structure and development of gynoecium from early to mature stage with stigma, style, ovary containing ovules (b). The floral stages and their corresponding duration time were indicated according to Smyth et al.

After one hour post-inoculation (HPI), *Agrobacterium* cells had already entered the locule of developing gynoecium (c) but were absent in later-stage gynoecia containing developed placenta tissue (d). Between 6-9 HPI, more *Agrobacterium* cells were observed in the locule (e), even at it began to close (f). *Agrobacterium* was not detected in fully closed gynoecia (g).

At one day post-inoculation (DPI), *Agrobacterium* cells were detected in young closed ovaries (h) but not in older ovaries undergoing ovule development (i). At 3 DPI (j), *Agrobacterium* cells persisted in ovaries at late developmental stages. By 5 DPI, *Agrobacterium* cells were enriched around the micropyle (arrow) (k), though no mCherry2 signal was detected. At floral open stage after 6 DPI, *Agrobacterium* accumulated around the micropyle, and mCherry2 signal became visible (l and m).

Asterisks (*) indicate placenta tissue; arrowheads denote developing ovule; arrows indicate *Agrobacterium* located around micropyle. Panels (a to k) were merged channel images; panels (l and m) show GFP, mCherry2, DIC and merged views. Scale bar= 100 µm.

Figure 2

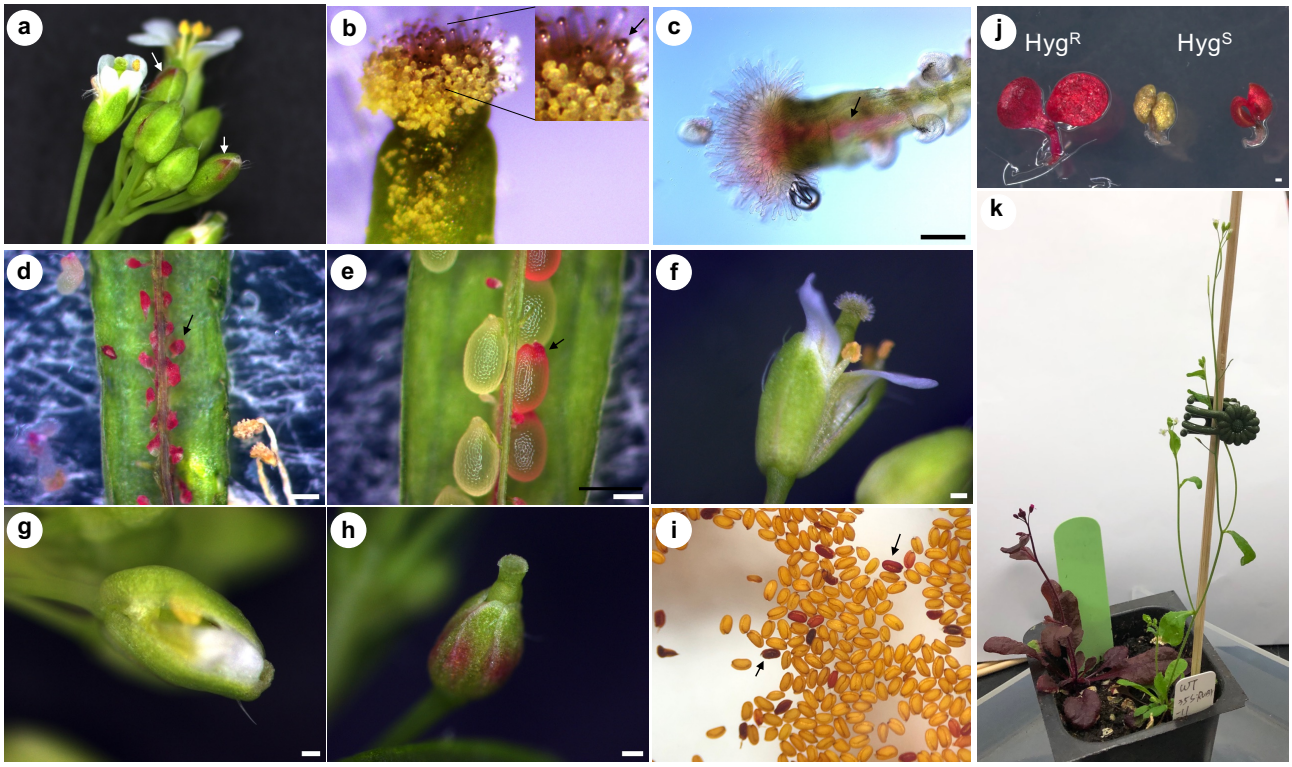

Figure 2. RUBY marker revealed transformation events in floral organs and female tissues
RUBY signals were observed in flowers (a), specifically on the stigma but not on pollen grains (b), and in the transmitting tissue (c). In siliques, RUBY expression was detected in both abortive (d) and developing ovules (e).

Flower morphology after AMT-FI ranged from normal open flowers (f) to partially open flowers (g), and flowers with only gynoecia emerging from sepals (h), all with visible RUBY signals.

RUBY signal intensity varied among seeds (i) and plants (j, k). (j) At the seedling stage, hygromycin-resistant (Hyg^R) and RUBY-positive seedling (left), non-transgenic seedling (middle), and RUBY-positive but hygromycin-sensitive (Hyg^S) seedling (right) were observed. (k) Transgenic T1 plants with variable RUBY expression patterns from strong whole-plant expression to undetectable signal. Scale bar = 200 µm.

Figure 3

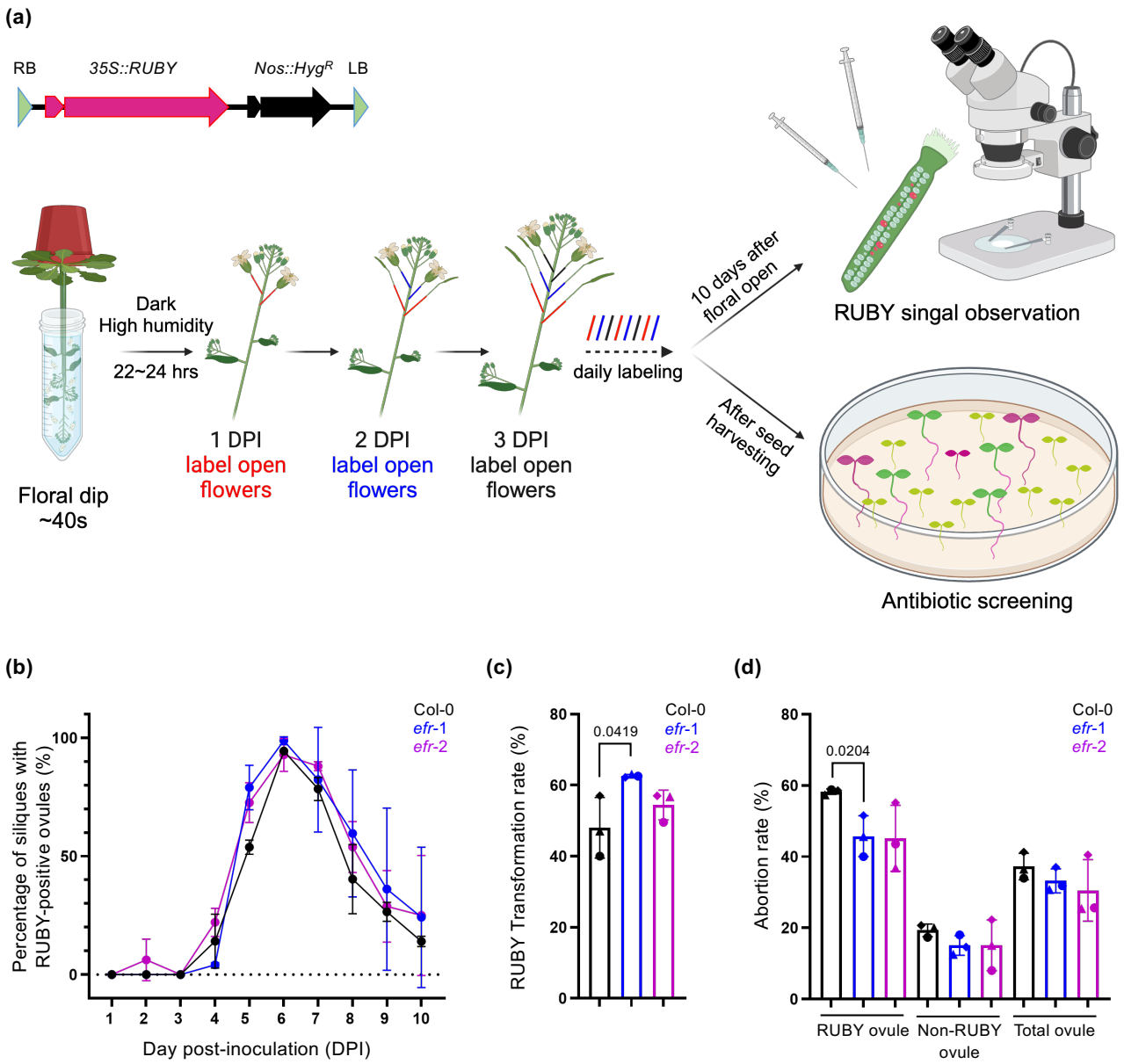

Figure 3. *Agrobacterium* infection and EFR-mediated immunity exert negative impacts on ovule development

(a) Experimental design: a schematic diagram illustrates the 35S::RUBY construct and experimental workflow. Transformation efficiency was evaluated based on the presence of RUBY-positive ovules and hygromycin-resistant seedlings.

(b) Percentage of siliques with RUBY-positive ovules recorded daily for Col-0 WT, *efr*-1, and *efr-2* from flowers that opened at 1-10 DPI. Data are mean ± SD of three biological replicates from representative of two independent experiments.

(c) RUBY-based transformation. Percentage of RUBY-positive ovules (include both developed and abortive ovules) per silique collected from flowers of Col-0 WT, *efr-1* and *efr-2* opened at 5-9 DPI was calculated (all data points shown in Fig. S2a). Data are mean ± SD of averaged percentage of RUBY-positive ovules from three independent experiments (circle, triangle and rhombus symbols). Statistically significant differences ($p < 0.05$) between Col-0 WT and efr mutants are indicated.

(d) Ovule abortion rate. The abortion rate of RUBY-positive, non-RUBY, and total ovules per silique collected from flowers of Col-0 WT, *efr*-1 and *efr*-2 opened at 5-9 DPI was calculated (all data points shown in Fig. S2c). Data are mean ± SD of averaged abortion rate from three independent experiments (circle, triangle and rhombus symbols). Statistically significant differences ($p < 0.05$) between Col-0 WT and efr mutants are indicated.

Figure 4

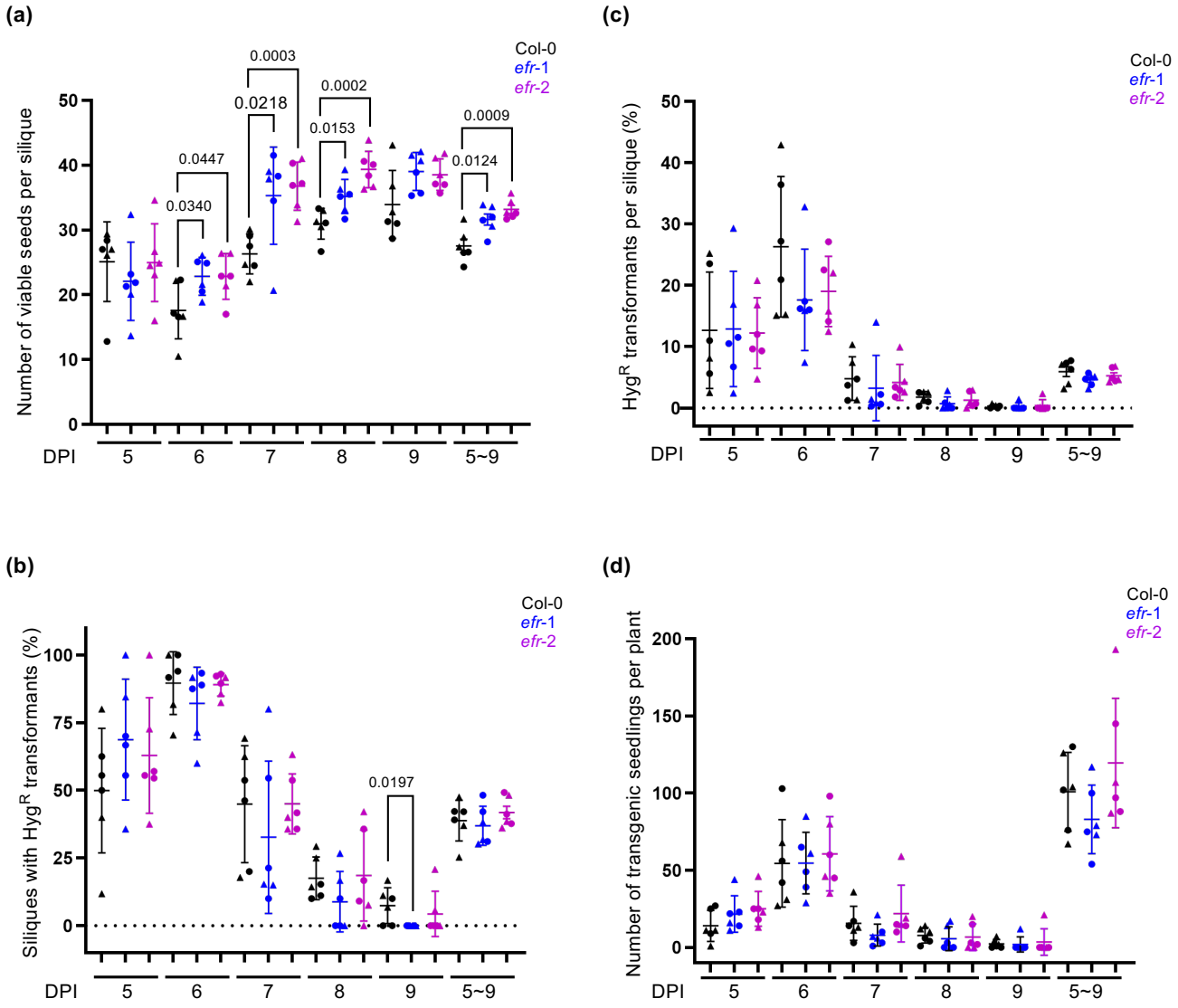

Figure 4. AMT events occur mainly in flowers opened at 5-9 DPI, peaking at 6 DPI

Siliques and seeds developed from flowers that opened at 5-9 DPI in Col-0 WT, *efr*-1 and *efr*-2 mutants were analyzed through viability (a) and hygromycin resistance (Hyg^R) screening (b, c, d) and viability (d). Data are (a) number of viable seeds per silique, (b) percentage of siliques containing Hyg^R transformants, (c) percentage of Hyg^R transformants per silique and (d) number of Hyg^R transformants per plant. Data are mean ± SD of six biological replicates from two independent experiments (circle and triangle symbols). Statistically significant differences ($p < 0.05$) between Col-0 WT and *efr* mutants are indicated.

Figure 5

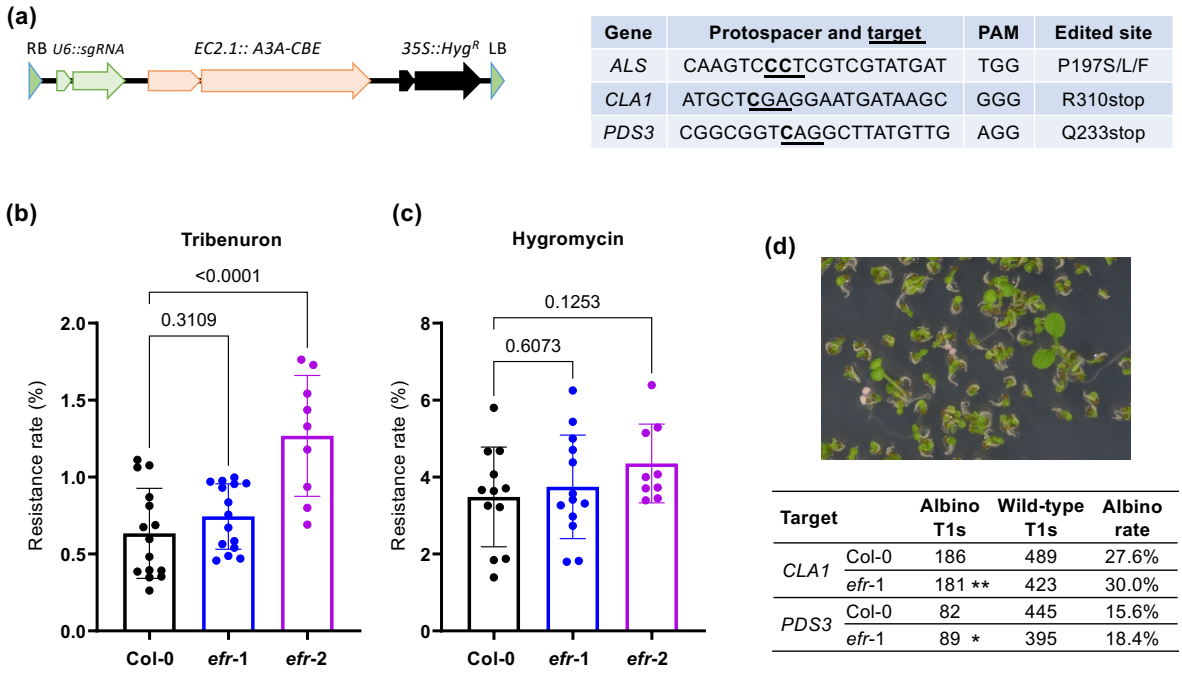

Gene	Protospacer and target	PAM	Edited site
ALS	CAAGTC**CC**TCGTCGTATGAT	TGG	P197S/L/F
CLA1	ATGCT**C**GAGGAATGATAAGC	GGG	R310stop
PDS3	CGGCGGT**C**AGGCTTATGTTG	AGG	Q233stop

Target		Albino T1s	Wild-type T1s	Albino rate
CLA1	Col-0	186	489	27.6%
	efr-1	181 **	423	30.0%
PDS3	Col-0	82	445	15.6%
	efr-1	89 *	395	18.4%

Figure 5. EFR suppresses genome editing efficiency

Agrobacterium GV3101 carrying a binary vector encoding a base editor and a sgRNA was used for floral inoculation in Col-0 WT and *efr* mutants to assess genome editing and stable transformation efficiencies. (a) A schematic diagram of the binary vector structure for base editing and target gene information. (b) Genome editing efficiency assessed by tribenuron-resistant T1 plants with targeting the *ALS* Pro197 locus. (c) Stable transformation efficiency evaluated by hygromycin resistance. Seeds are collected from flowers that opened at 5-9 DPI. Data are mean ± SD, with *p*-values calculated by Student's t-test between Col-0 WT and *efr* mutants. (d) Genome editing efficiency assessed based on albino phenotype in T1 plants, resulting from by loss-of-function mutations at locus *CLA1 and PDS3.* Statistically significant differences between Col-0 WT and *efr* are indicated (*$p < 0.05$, **$p < 0.01$, chi-square analysis).

Figure 6

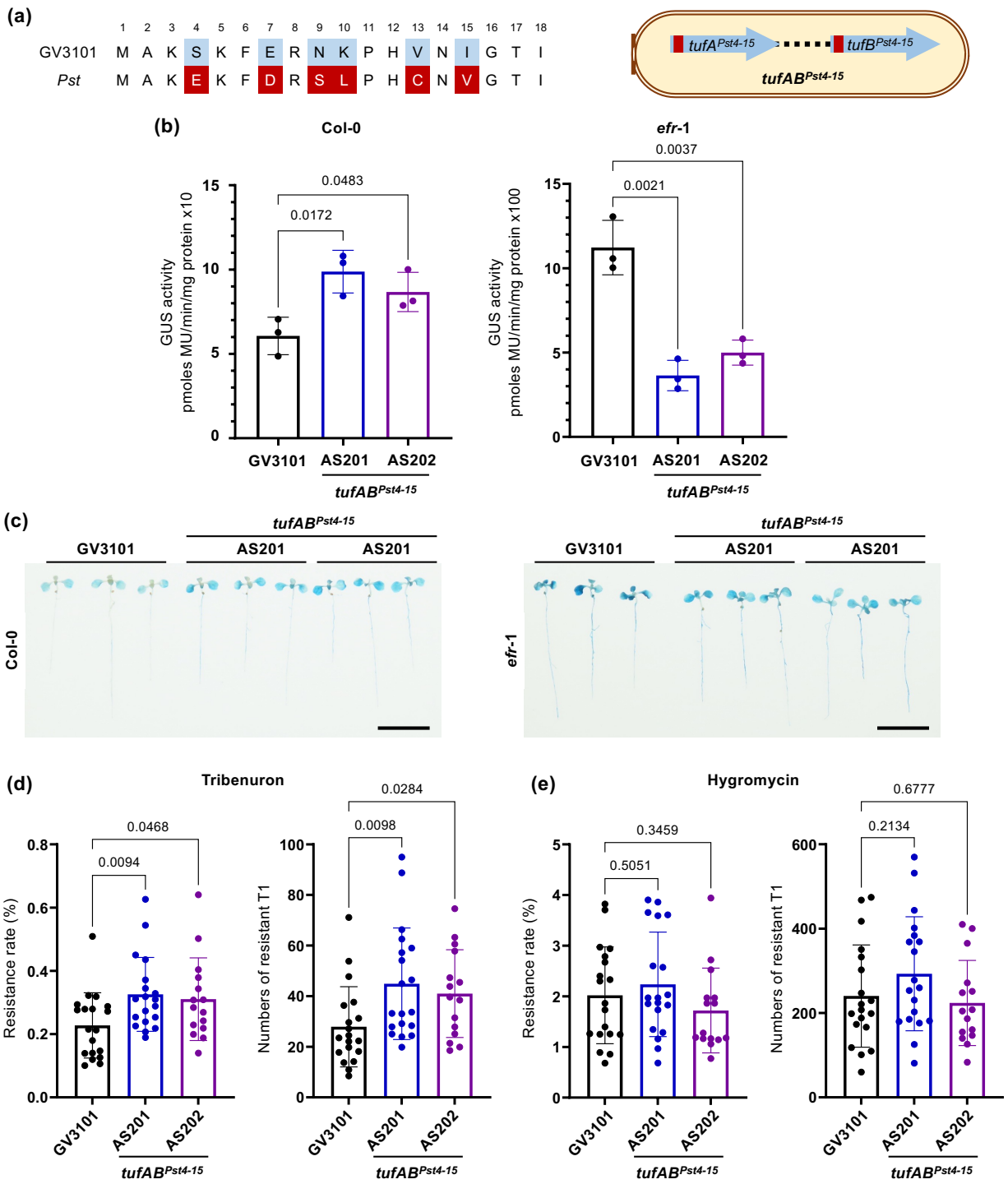

Figure 6. Modification of *Agrobacterium* EF-Tu enhances transient gene expression and genome editing efficiency but not stable T-DNA integration efficiency

The two engineered *Agrobacterium tufAB*$^{Pst4-15}$ strains, AS201 and AS202, were assessed for its efficiency in transient expression, genome editing, and stable transformation in comparison to the parental *Agrobacterium* GV3101.

(a) A schematic diagram illustrating the difference of *tufAB* sequences at amino acids 4th to 15th between *Agrobacterium* GV3101 and *Pseudomonas syringae* (*Pst*).

(b, c) Comparison of transient transformation efficiencies between the GV3101 WT and two *tufAB*$^{Pst4-15}$ strains (AS201 and AS202) in *A. thaliana* seedlings by quantitative GUS activity (b) GUS staining (c, scale bar =1 cm). Results are representative of three independent experiments.

(d) Comparison of genome editing efficiency between the GV3101 WT and two *tufAB*$^{Pst4-15}$ strains (AS201 and AS202) measured by the percentage of tribenuron-resistant T1 plants (left) and number of edited T1 plants per three T0 plants (right).

(e) Comparison of stable transformation efficiency by the number of hygromycin-resistant T1 plants per three T0 plants, with no significant differences between WT GV3101 and the two *tufAB*$^{Pst4-15}$ strains (AS201 and AS202).

Seeds were collected from all flowers. Each data point represents biological replicates from three independent experiments. All values are shown as mean ± SD, with *p*-values calculated by Student's t-test.

Figure 7

(a)

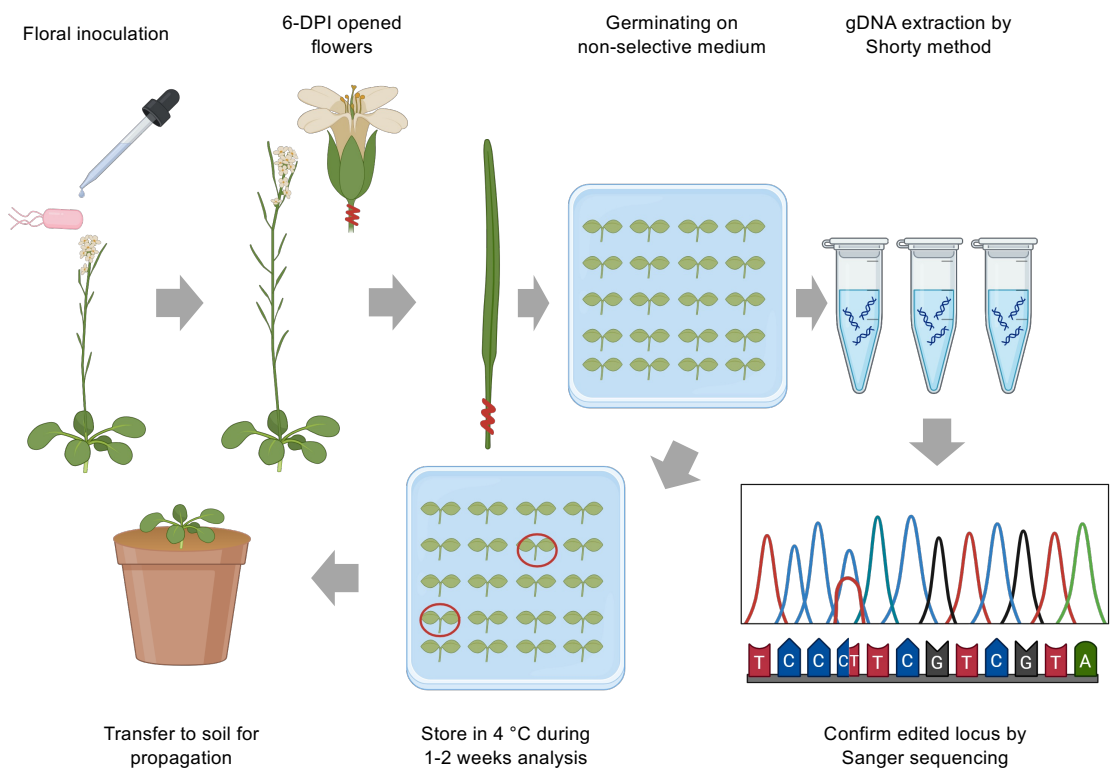

(b)

Plants	Col-0	*efr*-1	*efr*-2	Col-0	*efr*-1	*efr*-2	Col-0	Col-0
AMT-FI strain	GV3101	GV3101	GV3101	GV3101	GV3101	GV3101	GV3101	AS201
Target	*CLA1*	*CLA1*	*CLA1*	*CLA1*	*CLA1*	*CLA1*	*ALS*	*ALS*
Numbers of analyzed T1	212	188	236	64	63	64	94	93
GE confirmation	Albino seedling			Sanger sequencing			Sanger sequencing†	
Numbers of edited T1	7	7	10	1	10*	3	1	2
GE rate	3.30%	3.72%	4.24%	1.56%	15.87%	4.69%	1.06%	2.15%

Figure 7. Sequencing-based screening of genome-edited plants

(a) Workflow for screening genome-edited T1 plants from flowers that opened at 6 DPI. Seeds were germinated in 1/2 MS medium with only supplemented with timentin to suppress *Agrobacterium* growth without hygromycin selection. 10-day-old T1 plants were analyzed by Sanger sequencing at the *ALS* or *CLA1* loci.

(b) The number of sequenced T1 plants and editing rates. †indicates the C to T editing at Pro197 locus conferring tribenuron resistance. Statistically significant differences in genome editing (GE) rates between *efr-1* and WT Col-0 are indicated (* $p < 0.001$, chi-square analysis).

Supplemental figure 1

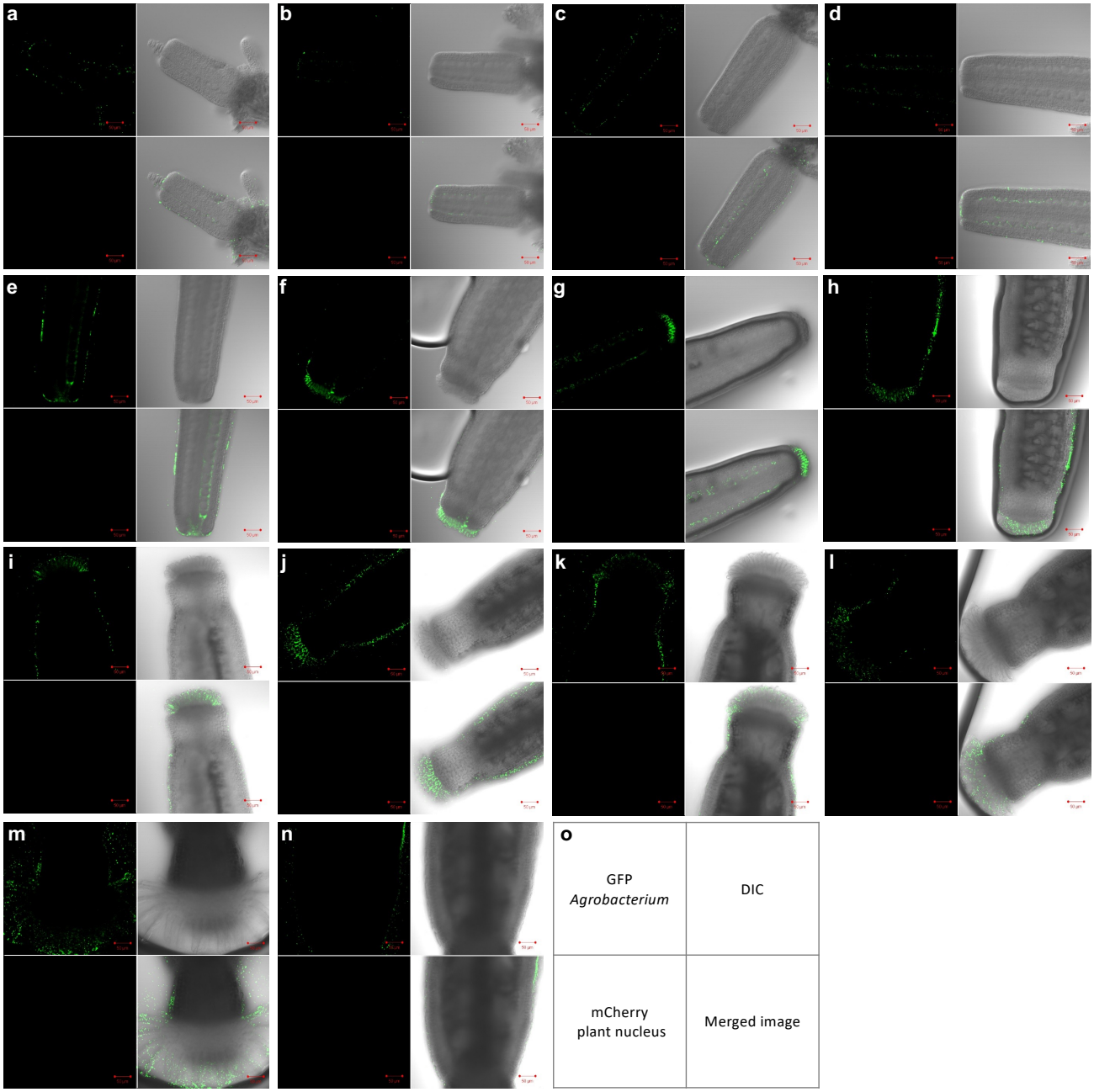

Figure S1. Basipetal analysis of *Agrobacterium* distribution along Arabidopsis inflorescence at 1 DPI.
A basipetal series of flowers from the inflorescence tip (a) to the first open flower at the base (m and n) were dissected to visualize *Agrobacterium* expressing GFP reporter at 1 DPI. Figures (m) and (n) are from different regions of the same flower. Each figure consists of four imaging channels (o). Scale bars indicated 50 µm.

Supplemental figure 2

(a)

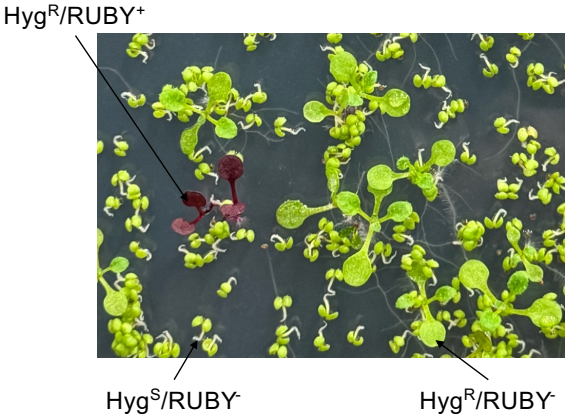

(b)

Genotype	Number of Hyg^{R} T1		
	Total	RUBY^{+}	Percentage of RUBY^{+}
Col-0 WT #1	67	4	6.0%
Col-0 WT #2	89	6	6.7%
Col-0 WT #3	48	3	6.3%
efr-1 *#1*	124	11	8.9%
efr-1 *#2*	129	15	11.6%
efr-2 *#1*	107	7	6.5%
efr-2 *#2*	117	11	9.4%

Figure S2. Number and percentage of Hyg^{R}/RUBY^{+} T1 seedlings.
(a) Representative photo of T1 seedlings screening on hygromycin containing 1/2 MS plate. The hygromycin-resistant T1 exhibiting RYBY signals of whole seedling (Hyg^{R}/RUBY^{+}) was indicated, among the hygromycin-resistant green and larger T1 seedling (Hyg^{R}/RUBY^{-}), and hygromycin-sensitive green but small seedlings (Hyg^{s}/RUBY^{-}). The hygromycin-sensitive T1 seedlings with RUBY signals (Hyg^{s}/RUBY^{+}) shown in Fig. 2j are rarely occurred and not present in this photo.

(b) Number and percentage of Hyg^{R}/RUBY^{+} T1 seedlings in Col-0 WT and *efr* mutants. Total number of Hyg^{R} T1 seedlings (Total) and those exhibiting RYBY signals of whole seedling (RUBY^{+}) was indicated and the percentage of Hyg^{R}/RUBY^{+} T1s among total Hyg^{R} T1s.

Supplemental figure 3

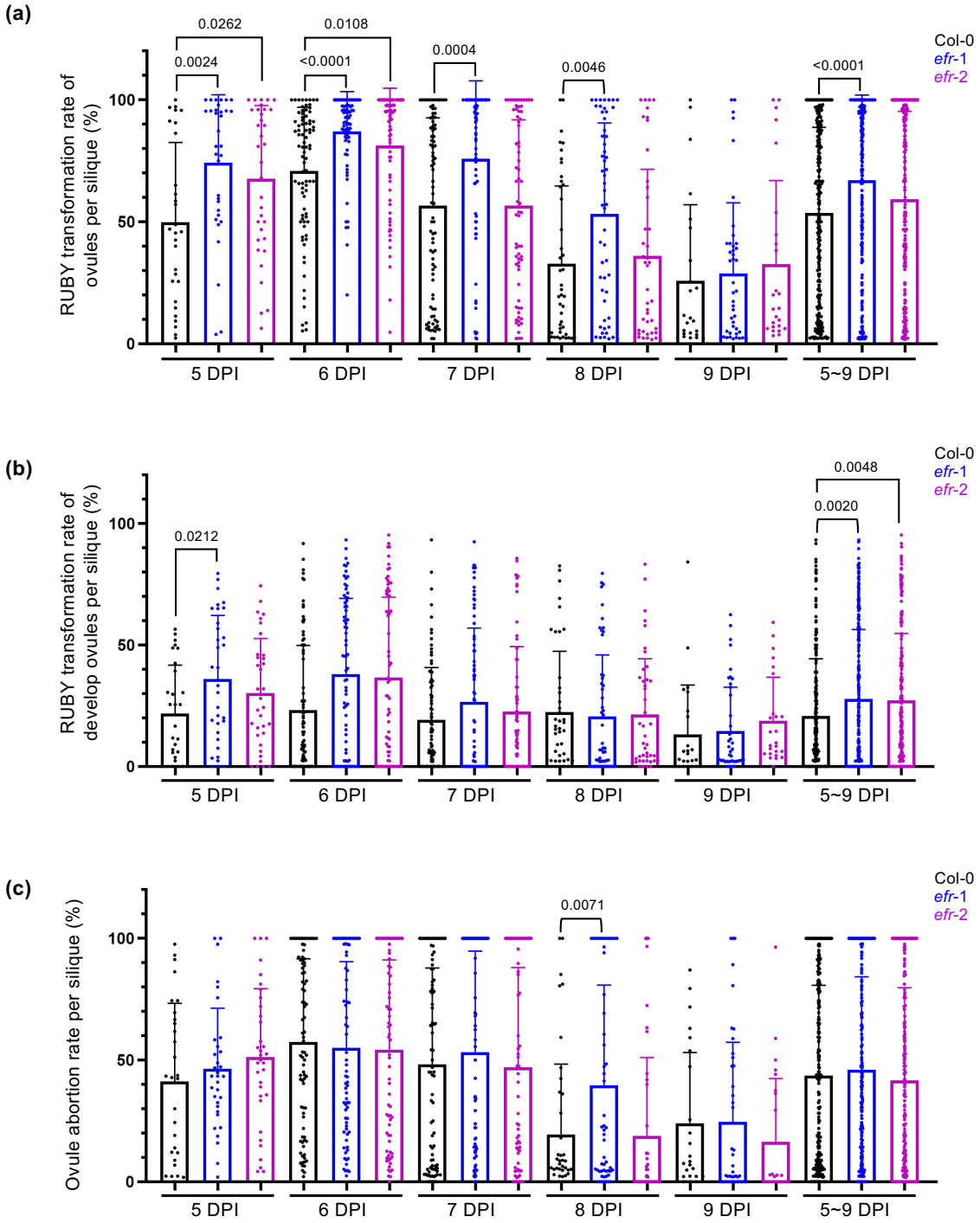

Figure S3. EFR-mediated immunity exerts negative impacts on ovule development and RUBY-based transformation rate

GV3101 carrying the 35S::RUBY construct was used for AMT-FI to assess RUBY-based transformation efficiency and ovule abortion rate in Col-0 WT and *efr* mutants. Siliques from flowers that opened at 5-9 DPI were analyzed to count the total number of ovules, the number of developed ovules with or without RUBY signals, and the number of abortive ovules with or without RUBY signals per silique. Related to Figure 3.

(a) Daily RUBY-based transformation rate per silique. The percentage of RUBY-positive ovules (including both developed and abortive ovules) per silique was calculate at each DPI, as well as cumulatively across 5-9 DPI. Each data point represents the percentage of RUBY-positive ovules per silique.

(b) Daily RUBY-based transformation rate of developed ovules per silique. The percentage of RUBY-positive developed (non-abortive) ovules per silique was measured at each DPI, as well as cumulatively across 5-9 DPIs. Each data point represents the percentage of RUBY-positive developed ovules per silique.

(c) Daily ovule abortion rate per silique. The percentage of abortive ovules (including both RUBY-positive and RUBY-negative) per silique was recorded at each DPI and cumulatively across 5-9 DPI. Each data point represents the percentage of abortive ovules per silique.

Data are shown in mean ± SD from three independent experiments, with p values calculated by Student's t-test between Col-0 WT and *efr* mutants.

Supplemental figure 4

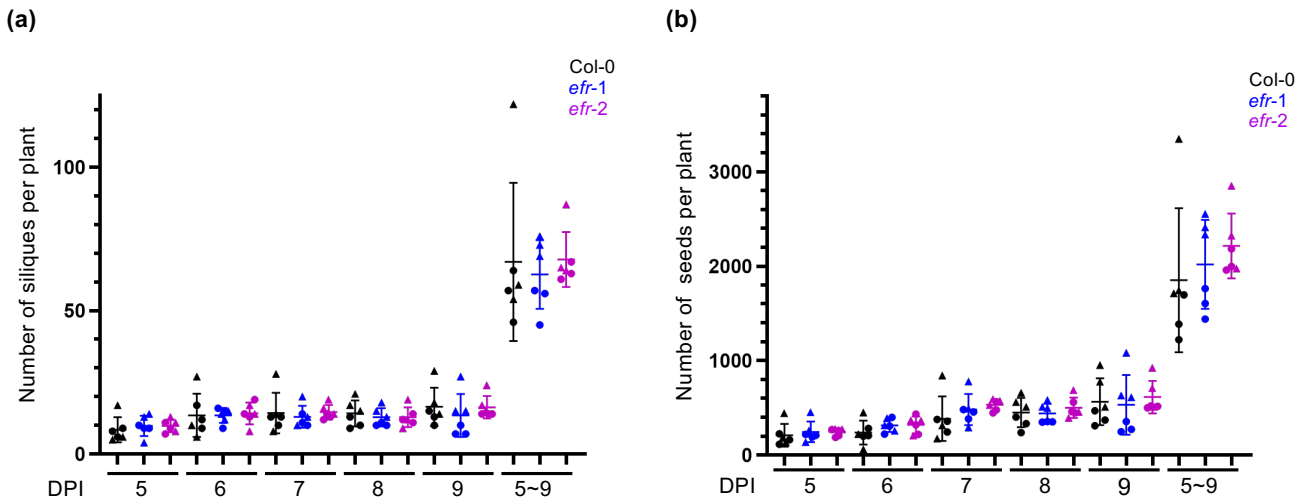

Figure S4. Silique and seed number in Col-0 WT, *efr*-1 and *efr*-2 mutants after AMT-FI.

Number of siliques (a) and seeds (b) developed from flowers that opened at 5-9 DPI per plant in Col-0 WT, *efr*-1 and *efr*-2 mutants were analyzed. Data are mean ± SD of six biological replicates from two independent experiments (circle and triangle symbols).

Supplemental figure 5

(a)

Number of Developed Seeds							Percentage of Developed Seeds after infection		
Treatment	Infiltration Medium (IM)			IM+GV3101					
Genotype	Col-0	*efr*-1	*efr*-2	Col-0	*efr*-1	*efr*-2	Col-0	*efr*-1	*efr*-2
Mean	35.6	42.7	44.5	29.4	37.4	40.6	82.6%	87.6%	91.2%
SD	13.1	9.2	11.0	16.3	14.0	12.8			
Number of Germinated Seeds (Germination Rate)							**Percentage of Germinated seeds after infection**		
Treatment	Infiltration Medium (IM)			IM+GV3101					
Genotype	Col-0	*efr*-1	*efr*-2	Col-0	*efr*-1	*efr*-2	Col-0	*efr*-1	*efr*-2
Mean	35.5 (99.7%)	42.5 (99.5%)	44.3 (99.6%)	26.4 (89.8%)	34.4 (92.0%)	36.7 (90.4%)	74.4%	80.9%	82.8%
SD	13.2	9.2	11.1	17.9	15.5	14.4			

(b)

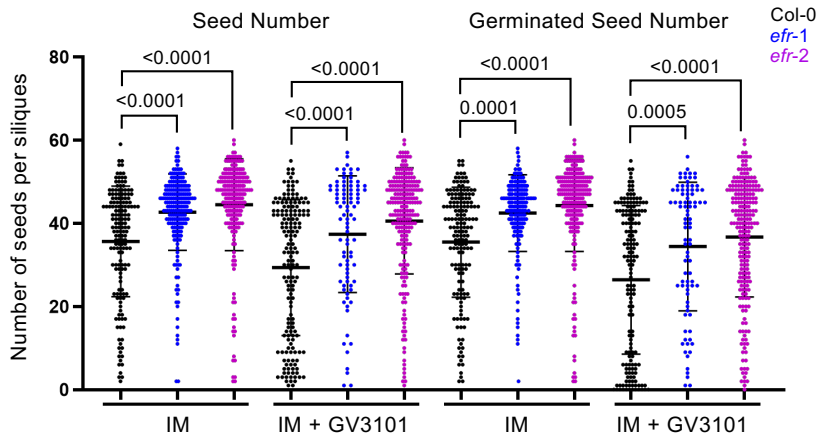

Figure S5. *Agrobacterium* infection and EFR-mediated immunity affect seed outputs

(a) Table showing seed number per silique from plants treated with infiltration medium alone or with *Agrobacterium.* Percentages of developed and germinated seeds after *Agrobacterium* infection, indicating the impact on seed viability.
(b) Seed counts and germination rates following infiltration medium alone (IM) or with *Agrobacterium* IM (IM + GV3101) treatments. Siliques were collected from flowers that opened at 5–9 DPI.

The total number of seeds and the number of germinated seeds were compared between treatments. Data were collected from two plants per genotype, except for *efr-1* infected with GV3101, where data were obtained from one plant. Data are shown as mean ± SD, with *p*-values calculated using Student's *t*-test to compare Col-0 WT and *efr* mutants.

Supplemental Table 1. Strain and Plasmid information

Lab collection #	***Agrobacterium* strain**/ Plasmid/ Antibiotics resistance	Characteristics	Source
EML485	**GV3101**/Rif^{R}Gen^R	GV3101 containing pMP90, which is pTiC58 derivative with T-DNA deletion and gentamicin resistance gene	Koncz and Schell, 1986
EML8561	**AS201**/ Rif^{R}Gen^R	GV3101::*tufAB*$^{Pst4-15}$ mutant by modifying *tufB* followed by *tufA*, with both genes encoding a chimeric EF-Tu with amino acids 4-15 from corresponding *Pst* EF-Tu	This study
EML8559	**AS202**/ Rif^{R}Gen^R	GV3101::*tufAB*$^{Pst4-15}$ mutant by modifying *tufA* followed by *tufB*, with both genes encoding a chimeric EF-Tu with amino acids 4-15 from corresponding *Pst* EF-Tu	This study
EML3375	pRL662-GFP(S65T)/ Gen^R	Broad host range plasmid confers gentamycin resistance and expression of GFP(S65T)	Yu et al., 2021
EML6428	pRL662-GFP(S65T)/Spe^R	Broad host range plasmid confers spectinomycin resistance and expression of GFP(S65T)	This study
EML6409	35S::RUBY/Spe^R	Binary vector carrying T-DNA expressing RUBY reporter and hygromycin resistance	Addgene#160908
EML6442	35S:mCherry2-NLS/Kan^R	Binary vector carrying T-DNA expressing mCherry2 florescent proteins	This study
EML8357	pA3A-CBECas9/Kan^R	Binary vector carrying T-DNA expressing base editor driven by egg-cell specific promoter	This study
EML8359	pA3A-CBECas9-Pro197/Kan^R	Binary vector carrying T-DNA expressing base editor targeting *ALS Pro197* locus	This study
EML8532	pA3A-CBECas9-CLA1/Kan^R	Binary vector carrying T-DNA expressing base editor targeting *CLA1*, generating early stop codon	This study
EML8533	pA3A-CBECas9-PDS3/Kan^R	Binary vector carrying T-DNA expressing base editor targeting *PDS3*, generating early stop codon	This study
EML121	pJQ200KS/Gen^R	Suicide plasmid contains *sacB* and Gm^R *traJ oriT* for the selection of double crossover events	Quandt and Hynes, 1993
EML8543	pEML041003/Kan^R	pJQ200KS derived suicide vector for gene replacement in *Agrobacterium*	This study
EML8552	pEML041003-tufAPst4-15/ Kan^R	Suicide vector for replacing 4th to 15th amino acids of *tufA*	This study
EML8553	pEML041003-tufBPst4-15/ Kan^R	Suicide vector for replacing 4th to 15th amino acids of *tufB*	This study

Gen^R, gentamycin resistance; Kan^R, kanamycin resistance; Rif^R, rifampicin resistance; Spe^R, spectinomycin resistance

Supplemental Table 2. Primer information

Primers	5' to 3' sequence	R.E. site	Source
Cloning of pRL662-GFP(S65T) with spectinomycin resistance			
Spe_F	GTCGATGTTTGATGTTATGGAGCAGCAACGATGGGGGAAGCGGTGATCGCCGAAGTATCG		This study
Spe_R	CGGGAAGCCGATCTCGGCTTGAACGAATTGTTATTTGCCGACTACCTTGGTGATCTCGCC		
662_F	CGATACTTCGGCGATCACCGCTTCCCCCATCGTTGCTGCTCCATAACATCAAACATCGAC		This study
662_R	GGCGAGATCACCAAGGTAGTCGGCAAATAACAATTCGTTCAAGCCGAGATCGGCTTCCCG		
Cloning of binary vector with 35S:mCherry2-NLS			
MC2-F	AAGGTCTCAAATGGTGAGTAAAGGAGAAGA	BsaI	This study
MC2-R	AAGGTCTCAAAGCTTAGGCGCCTACCTTTCTCTTCTTTTTTGGGCCTTTGTATAGTTCATCCATGCCACC	BsaI	
Cloning of protospacer			
Pro197-fw	ATTG CAAGTCCCTCGTCGTATGAT		Chen et al., 2017
Pro197-rv	AAAC ATCATACGACGAGGGACTTG		
CLA1-fw	ATTG ATGCTCGAGGAATGATAAGC		Liu et al., 2022
CLA1-rv	AAAC GCTTATCATTCCTCGAGCAT		
PDS3-fw	ATTG CGGCGGTCAGGCTTATGTTG		Liu et al., 2022
PDS3-rv	AAAC CAACATAAGCCTGACCGCCG		
Double crossover vector for cloning *tufA*$^{Pst4\text{-}15}$ and *tufB*$^{Pst4\text{-}15}$			
tufA-1f	TTGGTCTCAGGAGCACGATCTTGCGGATGC	BsaI	This study
tufA-1r	AGGTCTCGCCCTCCCGCATTGCAACGTCGGCACGATCGGTCACGTCG	BsaI	
tufA-2f	AGGTCTCGAGGGAACGATCAAATTTTTCCTTTGCCATGTGAATTGCTTCC	BsaI	
tufA-2r	AAGGTCTCGAGCGCAGTTCCGTCCACATCTTC	BsaI	
tufB-1f	TTGGTCTCAGGAGTTAGAGCTTGATTTCCACGTCAA	BsaI	
tufB-1r	AGGTCTCGCCCTCCCGCATTGCAACGTCGGCACGATCGGTCACGTCG	BsaI	
tufB-2f	AGGTCTCGAGGGAACGATCAAATTTTTCCTTTGCCATTAGTGGCTCTCC	BsaI	
tufB-2r	AAGGTCTCGAGCGTTCGAACCGAACCCTGA	BsaI	

References

Chen, Y., Wang, Z., Ni, H., Xu, Y., Chen, Q. and Jiang, L. (2017) CRISPR/Cas9-mediated base-editing system efficiently generates gain-of-function mutations in *Arabidopsis*. *Sci. China Life Sci.* **60**, 520-523.

Koncz, C. and Schell, J. (1986) The promoter of TL-DNA gene 5 controls the tissue-specific expression of chimaeric genes carried by a novel type of *Agrobacterium* binary vector. *Molec. Gen. Genet.* **204**, 383-396.

Liu, D., Xuan, S., Prichard, L.E., Donahue, L.I., Pan, C., Nagalakshmi, U., Ellison, E.E., Starker, C.G., Dinesh-Kumar, S.P., Qi, Y. and Voytas, D.F. (2022) Heritable base-editing in *Arabidopsis* using RNA viral vectors. *Plant Physiol.* **189**, 1920-1924.

Quandt, J. and Hynes, M.F. (1993) Versatile suicide vectors which allow direct selection for gene replacement in Gram-negative bacteria. *Gene* **127**, 15-21.

Yu M, Wang YC, Huang CJ, Ma LS, Lai EM. 2021. *Agrobacterium tumefaciens* deploys a versatile antibacterial strategy to increase its competitiveness. J Bacteriol 203:10.1128/jb. 00490-20.